Geosci. Model Dev., 8, 409–429, 2015
www.geosci-model-dev.net/8/409/2015/
doi:10.5194/gmd-8-409-2015


Geoscientific Model Development
Open Access

# A new WRF-Chem treatment for studying regional-scale impacts of cloud processes on aerosol and trace gases in parameterized cumuli

**L. K. Berg[1], M. Shrivastava[1], R. C. Easter[1], J. D. Fast[1], E. G. Chapman[1], Y. Liu[1], and R. A. Ferrare[2]**

[1]Pacific Northwest National Laboratory, Richland, WA, USA
[2]NASA Langley Research Center, Hampton, VA, USA

*Correspondence to:* L. K. Berg (larry.berg@pnnl.gov)

Received: 18 February 2014 – Published in Geosci. Model Dev. Discuss.: 29 April 2014
Revised: 23 January 2015 – Accepted: 28 January 2015 – Published: 24 February 2015

**Abstract.** A new treatment of cloud effects on aerosol and trace gases within parameterized shallow and deep convection, and aerosol effects on cloud droplet number, has been implemented in the Weather Research and Forecasting model coupled with Chemistry (WRF-Chem) version 3.2.1 that can be used to better understand the aerosol life cycle over regional to synoptic scales. The modifications to the model include treatment of the cloud droplet number mixing ratio; key cloud microphysical and macrophysical parameters (including the updraft fractional area, updraft and downdraft mass fluxes, and entrainment) averaged over the population of shallow clouds, or a single deep convective cloud; and vertical transport, activation/resuspension, aqueous chemistry, and wet removal of aerosol and trace gases in warm clouds. These changes have been implemented in both the WRF-Chem chemistry packages as well as the Kain–Fritsch (KF) cumulus parameterization that has been modified to better represent shallow convective clouds. Testing of the modified WRF-Chem has been completed using observations from the Cumulus Humilis Aerosol Processing Study (CHAPS). The simulation results are used to investigate the impact of cloud–aerosol interactions on regional-scale transport of black carbon (BC), organic aerosol (OA), and sulfate aerosol. Based on the simulations presented here, changes in the column-integrated BC can be as large as −50 % when cloud–aerosol interactions are considered (due largely to wet removal), or as large as +40 % for sulfate under non-precipitating conditions due to sulfate production in the parameterized clouds. The modifications to WRF-Chem are found to account for changes in the cloud droplet number concentration (CDNC) and changes in the chemical composition of cloud droplet residuals in a way that is consistent with observations collected during CHAPS. Efforts are currently underway to port the changes described here to the latest version of WRF-Chem, and it is anticipated that they will be included in a future public release of WRF-Chem.

## 1 Introduction/motivation

There remains a significant amount of uncertainty related to both the aerosol direct forcing and aerosol indirect effects (e.g., Solomon et al., 2007; Boucher et al., 2013). Numerical models of the atmosphere are one of the common tools used to investigate these effects. High-resolution simulations using horizontal grid spacing less than 10 km, which can explicitly represent convective clouds and cloud–aerosol interactions, have been widely used for short-term studies of cloud–aerosol interactions (e.g., Qian et al., 2009; Wang et al., 2011; Fan et al., 2012). They have not, however, generally been used for long-term simulations because of the associated computational expense. For long-term simulations, coarser horizontal resolution is generally required that necessitates the use of a cumulus parameterization even if the cloud–aerosol interactions associated with sub-grid-scale convective clouds are poorly represented (e.g., Zhao et al., 2011). Thus, treatments of aerosols in cumulus parameterizations are needed for investigations of the impact of clouds on aerosol mixing, transformation, and removal as well as the impact of aerosol on cloud properties (Stevens and Feingold, 2009).

Shrivastava et al. (2013) compared changes in the aerosol chemical composition and cloud microphysical structure associated with cloud–aerosol interactions in fields of shal-

low cumuli to data collected during the Cumulus Humilis Aerosol Processing Study (CHAPS; Berg et al., 2009). The main goal of CHAPS was to find evidence of cloud–aerosol interactions in fields of shallow cumuli. The simulations presented by Shrivastava et al. (2013) were completed with sufficiently high resolution that a convective parameterization was not required, allowing them to investigate cloud–aerosol interactions in relatively small shallow clouds that would be sub-grid scale at coarser resolutions. Among their findings were systematic changes in the chemistry of activated particles and cloud microphysics within shallow cumuli. They found that nitric acid vapor uptake by cloud droplets led to increased nitrate content in the cloud droplet residuals. They also reported changes in cloud microphysical properties, with increases in cloud droplet number concentration (CDNC) and decreases in droplet effective radius with an increase in pollutant loading.

The Weather Research and Forecasting model coupled with Chemistry (WRF-Chem) (Grell et al., 2005; Fast et al., 2006) is frequently used to simulate conditions over a range of spatial scales and has been used to study a wide range of atmospheric phenomena associated with atmospheric chemistry and aerosols (e.g., McKeen et al., 2007; Ntelekos et al., 2009; Grell et al., 2011; Pfister et al., 2011; Ahmadov et al., 2012; Matsui et al., 2013). To date, however, the treatment of cloud–aerosol interactions has largely been limited to grid-resolved clouds, which can be convective clouds if the model resolution is sufficiently fine (e.g., Chapman et al., 2009; Saide et al., 2012; Zhang et al., 2013; Eidhammer et al., 2014; Mashayekhi and Sloan, 2014). This is the case for WRF coupled with the Community Atmospheric Model version 5 (CAM5; Neale et al., 2012) physics parameterizations, although cloud–aerosol interactions in convectively detrained stratiform clouds are treated (Ma et al., 2013). One exception is the recent modification of the Grell cumulus parameterization (Grell, 1993; Grell and Dévényi, 2002) to include aqueous chemistry using Community Multiscale Air Quality (CMAQ) routines and aerosol interactions in the conversion of cloud water to rainwater and the evaporation of rain (Grell and Freitas, 2014). Lim et al. (2013) added a treatment of aerosol activation to the Zhang–McFarlane parameterization (Zhang and McFarlane, 1995), while Zhao et al. (2013) modified the Kain–Fritsch scheme to better account for transport and wet scavenging of dust, but each of their modifications does not include treatment of aqueous chemistry in the clouds, nor have they been added to the publicly released version of WRF-Chem. To address this missing process, we have modified WRF-Chem to include treatments of a number of factors and processes important for accurately representing aerosol and trace gases within sub-grid convective clouds, including fractional coverage of active and passive clouds, vertical transport, activation and resuspension, wet removal, and aqueous chemistry for cloud-borne particles. The new parameterization uses the Model for Simulating Aerosol Interactions and Chemistry (MOSAIC; Zaveri et al., 2008) packages to represent the aerosol chemistry. This new treatment is important for including additional realism in regional-scale modeling studies that require the use of cumulus parameterizations when investigating the effects of clouds on aerosol and the effects of aerosol on clouds. It should be noted, however, that the modifications do not yet include feedbacks of aerosol on the amount of precipitation, or feedbacks between the cumulus microphysics and the radiation. These additions are topics for subsequent research.

The work presented here describes the implementation of a treatment of activation, vertical transport, aqueous chemistry, and wet removal for sub-grid parameterized convective clouds in WRF-Chem. Section 2 describes changes to both the standard cumulus parameterization and the treatment of processes affecting aerosol and trace gases in the sub-grid convective clouds. These changes include improved treatment of cloud fractions as well as treatment of cloud droplet number concentration, vertical transport, activation/resuspension, aqueous-phase chemistry, and wet removal. Section 3 provides a description of the WRF-Chem configuration, simulation design, and emissions data used in the study. The data used from CHAPS are presented in Sect. 4. An analysis of the WRF-Chem simulations is presented in Sect. 5. Rather than focusing on the CHAPS study area only, results are also presented from three different locations that were selected to highlight the performance of the model in situations with shallow and deep sub-grid convective clouds, and to document the impact on the regional-scale transport, cloud microphysics, and the chemical composition of cloud droplets.

## 2 Modifications to WRF-Chem

The primary goal of this effort has been to improve the representation of vertical transport, aqueous chemistry, wet removal, and aerosol effects on cloud droplet number in parameterized sub-grid convective clouds within WRF-Chem. To address this goal, a number of modifications shown schematically in Fig. 1 have been made to WRF-Chem in order to account for cloud–aerosol interactions within these clouds. These modifications include changes to the Kain–Fritch (KF) cumulus scheme (Kain and Fritsch, 1990; Kain, 2004) as well as changes designed to account for transport, transformation, and removal of aerosols and trace gases within sub-grid convective clouds.

The WRF-Chem model architecture separates physical processes involving sub-grid cumulus, microphysics for grid-resolved clouds, boundary-layer turbulence, and radiation from processes involving aerosol and trace gases. We have followed this separation, so that code changes involve both a cumulus physics routine that determines the presence of sub-grid convective clouds, their properties, and their impacts on heat, moisture, and momentum, and a separate cumulus aerosol and trace gas routine that treats vertical trans-

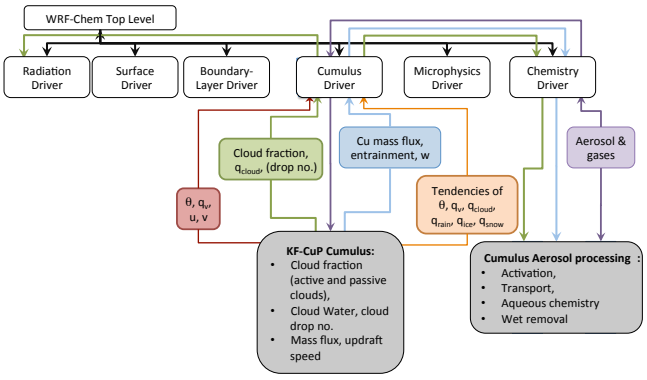


**Figure 1.** Summary of modifications to the standard implementation of WRF-Chem. Colored boxes indicate information passed between subroutines related to the thermodynamics (red), cloud microphysical and macrophysical properties (green), cloud dynamics (blue), thermodynamic tendencies (orange) and aerosol and trace gases (purple), while gray boxes indicate the new or modified parameterizations applied in WRF-Chem. Arrows indicate information flow within the model. Note that the droplet number generated in the KF–CuP parameterization is not currently used in the radiation driver.

port, activation/resuspension, aqueous chemistry, and wet removal of aerosol and trace gases. Modifications to the cumulus physics routine are described in Sects. 2.1.1, 2.1.2, and 2.2.1. The cumulus aerosol and trace gas routine, which is new to WRF-Chem, is described in Sect. 2.2.2.

The parameterization described in this work is an important first step in developing improved treatments of cloud–aerosol interactions and aqueous chemistry in sub-grid convective clouds. As such, the focus has been on capturing the first-order effects necessary for representing cloud–aerosol interactions and their impact on the aerosol life cycle. For this reason, a number of secondary processes were not incorporated during this first step, including direct scavenging of trace gases by rain, impaction scavenging of particles by rain, secondary activation, the effect of changing cloud droplet number concentration on radiation, and the second indirect effect. Each of these processes, however, can be added at a later date.

## 2.1 Modifications to the Kain–Fritsch cumulus parameterization

### 2.1.1 Trigger function for convection

Recently, the KF scheme has been modified to improve the treatment of shallow cumuli, which are defined by the KF scheme as being less than 2 to 4 km in height, depending on the temperature at the lifting condensation level. These changes were made primarily within the standard KF (Kain and Fritsch, 1990; Kain, 2004) convective parameterization and involved replacing the default ad hoc trigger function used in the parameterization with one explicitly linked to the boundary-layer turbulence. This was accomplished using the cumulus potential (CuP) scheme (Berg and Stull, 2005) leading to the new KF–CuP parameterization (Berg et al., 2013). These changes were designed to better account for sub-grid variability by applying a range of temperature and moisture perturbations from the grid-box mean as the convective trigger, thus allowing a population of shallow clouds with different thermodynamic properties to coexist in a model grid column. In the case of deep convection, only the single most probable temperature and moisture perturbation that triggered clouds is applied, to be consistent with the standard implementation of the KF scheme. The sub-grid distribution of temperature and humidity was parameterized using probability density functions (PDFs) of temperature and humidity that were based on the jump of potential temperature and moisture at the surface and at the boundary-layer top (Berg and Stull, 2004). These modifications, along with the cloud fraction changes (Sect. 2.1.2), were shown to significantly increase the frequency of occurrence of simulated shallow clouds over the Southern Great Plains, leading to improved forecasts of both cloud fraction and downwelling shortwave irradiance (Berg et al., 2013). It should also be noted that, while the new trigger function is not scale aware, it could easily be modified to adjust the PDF based on the model grid spacing.

### 2.1.2 Cloud fractional area

In their modifications to the standard KF scheme, Berg et al. (2013) included a simple treatment of the cloud fraction associated with sub-grid-scale convective clouds. Their method was based on representative timescales associated with cumulus, which the method defined as a function of the cloud depth, turbulence intensity, and moisture in the cloudy layer. In the work presented here, an additional treatment was added to determine the cloud fractional area for instances with deep convection. Rather than develop a new representation of the total cloud fraction for deep convection, the empirical treatment used in CAM5 is applied. In this parameterization, the cloud fraction associated with deep convection is a function of the convective mass flux (Neale et al., 2012), and is represented as

$$\sigma_{\mathrm{dp,cu}} = k_{1,\mathrm{dp}} \ln\left(1 + k_2 M_{\mathrm{dp,cu}}\right), \quad (1)$$

where $\sigma_{\mathrm{dp,cu}}$ is the cloud fraction associated with deep-convective clouds, $k_{1,\mathrm{dp}}$ is an adjustable parameter set to 0.1, $k_2$ is assumed to be 675, and $M_{\mathrm{dp,cu}}$ is the updraft mass flux of the convective clouds (in $\mathrm{kg\,m^{-2}\,s^{-1}}$). The values of both $k_{1,\mathrm{dp}}$ and $k_2$ were selected to be the same as the values used in CAM5, and are identical to those used by Ma et al. (2013) in their implementation of the CAM5 physics in WRF and made publically available in version 3.5, and are similar to that proposed by Alapaty et al. (2012) and Herwehe et al. (2014). It could be argued that a parameterization of cloud fraction developed for a relatively coarse-resolution model

like CAM5 is not appropriate for a regional-scale model like WRF, which can be run at a wide range of resolutions. The cloud fraction defined by Eq. (1) can vary with model grid spacing due to changes associated with $M_{\mathrm{dp,cu}}$, and as such has some scale dependence. When run at high horizontal resolution, however, the cumulus parameterization is generally turned off, so that the parameterization of sub-grid convective cloud fraction is not utilized. Given the constants defined above, Eq. (1) predicts the maximum cloud fraction in the grid cell associated with deep convection to be approximately 45 %. Similar to the methodology applied by Berg et al. (2013) for cases of shallow cumuli, the deep-cloud fraction computed using Eq. (1) is applied in the radiation parameterization but has no impact on either the convective tendencies for heat, moisture, and momentum, or on the cumulus transport of aerosols and trace gases. It is, however, used in the computations related to aqueous chemistry described in Sect. 2.2.

The cloud fraction associated with both shallow and deep sub-grid convective clouds is broken up further into two subtypes: active and passive clouds (e.g., Stull, 1985). Active clouds are those that have vigorous updrafts and contribute to the upward cloud mass fluxes. The fractional area of active cumulus for shallow clouds is defined as the fraction of the PDF of temperature and humidity applied in the convective scheme that forms clouds, while for deep clouds it is the standard KF updraft fraction area. Passive clouds consist primarily of decaying clouds without a well-organized updraft. The fractional area of the passive clouds is determined as the difference between the total cloud fraction (computed following Berg et al. (2013) for shallow clouds, and Eq. (1) for deep clouds) and the active cloud fraction that is determined within the KF–CuP scheme. Passive clouds are treated as quiescent and are assigned zero vertical velocity, so that there is no vertical mass flux. They are assumed to have the same total cloud water and ice content as the active clouds, but to be non-precipitating, so there is no wet removal associated with passive clouds. In addition, when a convective cloud is triggered in a model grid column, the cloud population is assumed to be in steady state over the cloud lifetime defined in the cumulus parameterization (30 min for shallow clouds and 30 to 60 min for deep clouds).

## 2.2 Modifications to account for vertical transport, aqueous chemistry, wet removal, and cloud droplet number

Chapman et al. (2009) described a treatment of cloud–aerosol interactions for grid-resolved clouds within WRF-Chem. For cloudy grid cells, the standard version of WRF-Chem treats both cloud-borne (activated) and interstitial (non-activated) particles as separate transported species. A number of modifications to the standard WRF-Chem version 3.2.1 have been implemented in this study to specifically address cloud–aerosol interactions in sub-grid convective clouds. These modifications include calculations for

- cloud droplet number mixing ratio,
- cloud microphysical (conversion rates, and cloud water and cloud ice mixing ratios) and cloud macrophysical properties (updraft fractional area, updraft and downdraft mass fluxes, and entrainment) averaged over the population of shallow convective clouds, or for the single deep convective cloud value, and
- vertical transport, activation/resuspension, aqueous chemistry, and wet removal of aerosols and trace gases.

WRF-Chem has several different aerosol and trace gas representations, which are referred to as chemistry packages. Our changes for sub-grid convective clouds were implemented with the MOSAIC (Zaveri et al., 2008) sectional aerosol model and the SAPRC-99 photochemical mechanism (Carter, 2010). Extension to other WRF-Chem chemistry packages would be relatively straightforward, especially those packages for which aqueous chemistry and aerosol activation modules (or interfaces) already exist.

### 2.2.1 Aerosol effects on the cloud droplet number

Within the default KF scheme, as well as other cumulus parameterizations applied in WRF, a highly simplified treatment of cloud microphysics is used. Cloud water is produced in updrafts and converted to precipitation based on a prescribed e-folding height, and additional assumptions are made involving frozen condensate and precipitation and detrainment to downdrafts (e.g., Kain and Fritsch, 1990). While such a simplified treatment has been successful for mesoscale weather forecasting, it is not sufficient for studying cloud–aerosol interactions that are intimately linked to the cloud microphysics. Thus, the activation of cloud droplets in convective drafts must be considered. The activation is a function of the cloud updraft speed and the number, size, and composition of particles. In the modified version of the KF parameterization in WRF-Chem that accounts for the cloud droplet number, the updraft velocities associated with the buoyancy excess are computed using the temperature and humidity perturbations for the range of parcels identified by the KF–CuP parameterization that form clouds. Furthermore, the droplet activation for each perturbation is computed by applying an entraining parcel conceptual model using the Abdul-Razzak and Ghan (2000) parameterization modified to account for entrainment following Barahona and Nenes (2007). Once the droplet number concentrations are computed for each perturbation value of temperature and humidity in the PDF, they are averaged together to provide a single value of cloud droplet number concentration for each grid cell. Above the cloud base, the number of cloud droplets is further reduced by entrainment, where the entrainment rates are determined using the KF scheme (averaged over all of the parcel perturbations

to yield a single entrainment rate). At present, secondary activation is not considered for either sub-grid convective clouds or for high-resolution (cloud-resolving) simulations of cumulus convection. In addition, the activation does not feedback on the cumulus clouds via changes in the conversion of cloud water to rain (as treated by Grell and Freitas, 2014).

#### 2.2.2 Effects of sub-grid cumulus on aerosol and trace gases

A new module was introduced to WRF-Chem to calculate the effects of sub-grid convective clouds on aerosol and trace gases, including vertical transport, activation/resuspension, aqueous chemistry in cloud droplets, and wet removal. The new module has separate sections that treat the active clouds (as well as vertical transport in the subsiding environment surrounding the active clouds) and passive clouds (for which the only process is aqueous chemistry).

In models of the cloud (and precipitation) effects on aerosols and trace gases, one must consider the attachment state (Ghan and Easter, 2006) of (aerosol) particles and gases. For example, interstitial aerosol particles (i.e., particles suspended in air) may become attached to, dissolved in, or suspended in various hydrometeors (cloud and rain drops, ice crystals, snow and graupel particles). When the aerosol representation involves several size bins (8 in our study) and multiple chemical species within each bin (14 in our study), the computational expense of explicitly treating all possible attachment states is considerable, and simplifying assumptions are often used. For example, in Chapman et al. (2009), the treatment of cloud–aerosol interactions focused on grid-resolved warm clouds. Aerosol material (sulfate, nitrate, etc.) associated with cloud droplets (referred to as cloud-borne) of grid-resolved clouds was treated explicitly as transported prognostic species, while moderately soluble gases dissolved in cloud droplets were assumed to be in equilibrium with the gas phase and were treated diagnostically. Aerosol material and gases that became associated with precipitation particles (rain, snow, graupel) and also ice crystals were assumed to be quickly removed from the atmosphere and were not treated explicitly. A similar but somewhat simpler approach is used in our treatment of sub-grid cumulus effects. For all attachment states, the aerosol species associated with cloud droplets in the sub-grid convective clouds are treated explicitly, but only within the convective cloud routines. This approximation is reasonable because of the relatively short lifetime of the parameterized convective clouds (30–60 min) and the fact that the parameterization is intended for use with model horizontal grid spacings of approximately 10 km or more. When air is detrained from sub-grid convective clouds, any detrained cloud-borne aerosol is added to the grid-resolved interstitial aerosol in that grid box where the aerosol can potentially interact with resolved clouds.

The cumulus physics routine determines whether sub-grid convective cloud is present within a model grid column and the physical properties of the cumulus clouds (shallow or deep; lifetime; updraft and downdraft mass fluxes, entrainment, and vertical velocity; mixing ratios of cloud water, ice, and precipitation; and microphysical conversion of cloud water to cloud ice and precipitation) that are used in the cumulus effects routine. Within the KF–CuP scheme, when deep convection is diagnosed within a grid column, the deep clouds are assumed identical, and there is a single vertical profile for updraft and downdraft mass fluxes and each microphysical parameter. When shallow convection is diagnosed, there is a population of shallow clouds with different profiles, and downdrafts are not treated. In the cumulus-effects-on-aerosols routine, calculations are made using the properties of an average (over the population) shallow cloud, rather than doing calculations for each shallow cloud in the population. In this study, the median coefficient of variability of the cloud-base vertical velocity for shallow sub-grid convective clouds was 0.11, and 78 % of all values were less than 0.25, which highlights the fact that the variability in the updraft strength within a grid cell is relatively small. This methodology is applied to limit the information that is passed between the various WRF-Chem modules, to reduce computational burden, and to allow the same treatment for shallow and deep cumuli. The changes in aerosol properties associated with aqueous chemistry and transport in the shallow clouds are less sensitive to the details of the population of cumulus updrafts than is the cloud droplet number concentration, and the largest impact is on the distribution of aerosol mass between the size bins (as determined by which bins are activated) rather than changes in the total aerosol mass.

Active cloud calculations are performed first, followed by passive cloud calculations. The treatment of active sub-grid cumulus effects on aerosols and gases is very similar to the unified treatment described in the supplementary material of Wang et al. (2013). The active-cloud updrafts and downdrafts are treated as steady-state entraining plumes. The updraft and downdraft mass fluxes obey

$$\frac{\partial M_Y}{\partial z} = \frac{(E_Y - D_Y)}{\Delta z}, \tag{2}$$

where the $Y$ subscript is either U for updraft or D for downdraft, $M_Y$ is the mass flux ($\mathrm{kg\,m^{-2}\,s^{-1}}$) defined at vertical layer boundaries, and $E_Y$ and $D_Y$ are the entrainment and detrainment in a layer, and $\Delta z$ is the layer thickness. The compensating mass flux in the environment, $M_\mathrm{E}$, is equal to $-(M_\mathrm{U}+M_\mathrm{D})$. The active-cloud calculations involve integrating conservation equations for grid-cell mean mixing ratios of aerosol and trace gas species over the lifetime of the cumulus cloud. The integration uses an internal time sub-step selected automatically so that the transport of air out of a layer (by $M_\mathrm{E}$, $E_\mathrm{U}$, and $E_\mathrm{D}$) during the sub-step does not exceed the layer's air mass $\rho\Delta z$, where $\rho$ is the air density.

For each time sub-step, steady-state vertical profiles of aerosol and trace gas species in the updraft and downdraft are first calculated. This is done by integrating steady-state con-

tinuity equations upwards (for updrafts) or downwards (for downdrafts). For aerosol species in the updraft, the continuity equation is

$$\frac{\partial\left(M_{\mathrm{U}}q_{X,\mathrm{U}}\right)}{\partial z}=\frac{\left(E_{\mathrm{U}}q_{X,\mathrm{E}}-D_{\mathrm{U}}q_{X,\mathrm{U}}\right)}{\Delta z} + \rho A_{\mathrm{U}}\left[\left(\dot{q}_{X,\mathrm{U}}\right)_{\mathrm{ACTI}}+\left(\dot{q}_{X,\mathrm{U}}\right)_{\mathrm{WETR}}+\left(\dot{q}_{X,\mathrm{U}}\right)_{\mathrm{AQCH}}\right]. \quad (3)$$

Here $q_{\mathrm{X,E}}$ and $q_{\mathrm{X,U}}$ are aerosol mixing ratios in the environment (E) and updraft (U), respectively, and the $X$ subscript is either AI for interstitial aerosol species or ACC for convective-cloud-borne (activated) aerosol species. The environment mixing ratios for interstitial aerosol are assumed equal to the grid-cell mean values, and are zero for convective-cloud-borne aerosol. $A_{\mathrm{U}}$ is the updraft fractional area and is equal to $(M_{\mathrm{U}}/\rho w_{\mathrm{U}})$, where $w_{\mathrm{U}}$ is the updraft vertical velocity. The last three terms on the right-hand side are the rates of change due to activation (ACTI), in-cloud wet removal (WETR), and aqueous-phase chemistry within cloud droplets (AQCH). For interstitial aerosol, only the activation term is non-zero.

Aerosol activation is calculated as described in Sect. 2.2.1, but with the simplification of using the average (over different clouds) vertical velocity for shallow cumuli rather than a range of values that is used in the cumulus physics routine (the reasons for this simplification were discussed earlier in this sub-section). The Abdul-Razzak and Ghan (2000) parameterization provides activation fractions ($f_{\mathrm{ACT}}$) for aerosol number and mass species in each size bin. The activation rate in Eq. (3) is then

$$\left(\dot{q}_{\mathrm{ACC,U}}\right)_{\mathrm{ACTI}}=-\left(\dot{q}_{\mathrm{AI,U}}\right)_{\mathrm{ACTI}}=\left(f_{\mathrm{ACT}}q_{\mathrm{AI,U}}\right)/\Delta t_{\mathrm{U}}, \quad (4)$$

where $\Delta t_{\mathrm{U}}=\Delta z/w_{\mathrm{U}}$ is the time for updraft air to move across a layer.

The wet removal rate for cloud-borne aerosol in Eq. (3) is given by

$$\left(\dot{q}_{\mathrm{ACC,U}}\right)_{\mathrm{WETR}}=-\left(f_{\mathrm{WETR}}q_{\mathrm{ACC,U}}\right)/\Delta t_{\mathrm{U}}, \quad (5)$$

where $f_{\mathrm{WETR}}$ is the fractional removal of cloud-borne aerosols in the updraft as they move across a layer. This fractional removal is currently equal to the fractional conversion of cloud water to precipitation across the layer, which is provided by the cumulus physics routine. Cloud water could also be converted to cloud ice in the cumulus physics routine, but currently this process is not included in the aerosol wet removal calculations. The conversion rate of cloud water to precipitation that is currently used in the cumulus physics routine is quite rapid, so in deep clouds, most cloud-borne aerosols are wet removed before reaching the detrainment level, and this simplification has little impact. However, this treatment is not ideal, and in the future, ice processes could be incorporated into the cumulus effects routine by treating cloud-ice-borne aerosol in addition to cloud-droplet-borne aerosol.

The aqueous-phase chemistry rate in Eq. (3) is obtained by calling the WRF-Chem cloud-chemistry routine for grid-resolved clouds (Chapman et al., 2009). This routine calculates mixing ratio changes from gas uptake and aqueous-phase reactions in an air parcel (or layer) over a specified time step, and it is applied to updraft air moving across a layer in time $\Delta t_{\mathrm{U}}$.

For trace gases in the updraft, the continuity equation is

$$\frac{\partial\left(M_{\mathrm{U}}q_{\mathrm{G,U}}\right)}{\partial z}=\frac{\left(E_{\mathrm{U}}q_{\mathrm{G,E}}-D_{\mathrm{U}}q_{\mathrm{G,U}}\right)}{\Delta z} + \rho A_{\mathrm{U}}\left[\left(\dot{q}_{\mathrm{G,U}}\right)_{\mathrm{WETR}}+\left(\dot{q}_{\mathrm{G,U}}\right)_{\mathrm{AQCH}}\right], \quad (6)$$

where $q_{\mathrm{G,E}}$ and $q_{\mathrm{G,U}}$ are gas mixing ratios in the environment and updraft, respectively. The environment gas mixing ratios are assumed equal to the grid-cell mean values, which is justified given the small fractional area of the grid box covered with convective updrafts. The $q_{\mathrm{G,U}}$ includes both gas-phase and dissolved in convective cloud-water species (e.g., gaseous $SO_2$ plus S(IV) in cloud water). The WRF-Chem cloud-chemistry routine gives the aqueous-phase chemistry rate in Eq. (6), as well as the fraction of the gas that is dissolved in convective cloud water ($f_{\mathrm{G,CCW}}$). The wet removal rate for gases only considers the removal of gases dissolved in cloud droplets, and direct uptake of gases by rain is currently neglected. This treatment is justified within clouds because of the relatively small role of direct uptake by raindrops compared to uptake by cloud droplets followed by droplet collection by rain (due to the small surface area of raindrops compared to cloud droplets). Also, the volume of air that moves through the updraft (and experiences in-cloud wet removal) is larger than the volume that resides below the cloud base but does not enter the updraft (and experiences only below-cloud wet removal). Future versions of the parameterization will include below-cloud wet removal. The wet removal rate in Eq. (6) is then

$$\left(\dot{q}_{\mathrm{G,U}}\right)_{\mathrm{WETR}}=-\left(f_{\mathrm{WETR}}f_{\mathrm{G,CCW}}q_{\mathrm{G,U}}\right)/\Delta t_{\mathrm{U}}. \quad (7)$$

Downdrafts are assumed to be sub-saturated and contain no cloud droplets or convective-cloud-borne aerosol. Thus, activation, wet removal, and aqueous-phase chemistry are not treated in downdrafts. The downdraft continuity equations are then

$$\frac{\partial\left(M_{\mathrm{D}}q_{X,\mathrm{D}}\right)}{\partial z}=\frac{\left(E_{\mathrm{D}}q_{X,\mathrm{E}}-D_{\mathrm{D}}q_{X,\mathrm{D}}\right)}{\Delta z}, \quad (8)$$

where $X$ is either AI for interstitial aerosol species or $G$ for gases.

Once the aerosol and gas profiles in the updraft and downdraft have been calculated, conservation equations for grid-cell mean mixing ratios of aerosol and trace gas species are integrated for the time sub-step. These conservation equa-

tions have the form

$$\rho \frac{\partial \overline{q}_X}{\partial t} = -\frac{\partial}{\partial z}\left[M_{\mathrm{U}} q_{X,\mathrm{U}} + M_{\mathrm{D}} q_{X,\mathrm{D}} + M_{\mathrm{E}} q_{X,\mathrm{E}}\right] + \rho A_{\mathrm{U}}\left[\left(\dot{q}_{X,\mathrm{U}}\right)_{\mathrm{ACTI}} + \left(\dot{q}_{X,\mathrm{U}}\right)_{\mathrm{WETR}} + \left(\dot{q}_{X,\mathrm{U}}\right)_{\mathrm{AQCH}}\right], \quad (9)$$

where the $X$ subscript is either AI, ACC, or $G$, and the updraft rate of change terms come from the updraft calculations described above. The integration is explicit in time and uses simple upstream finite differencing for the vertical transport terms. After the integration sub-step, the grid-cell mean mixing ratio of convective-cloud-borne aerosol ($\overline{q}_{\mathrm{ACC}}$) may be non-zero at or near levels where the updraft detrains. This convective-cloud-borne aerosol is partially transferred to grid-resolved cloud-borne aerosol (fraction transferred equal to grid-resolved cloud fraction) and partially resuspended to interstitial aerosol. At the end of all the active-cloud integration sub-steps, the new grid-cell mean aerosol and gas mixing ratios reflect the effect of the active cumulus cloud over the cloud lifetime.

The passive cumulus effects calculations are performed next. These calculations are relatively simple in comparison, as there is no vertical transport or wet removal of aerosol. The cumulus physics routine provides the passive cumulus cloud fraction and cloud water mixing ratio at each vertical level. Initial mixing ratios of interstitial aerosol and trace gases are set equal to the grid-cell mean mixing ratios at the end of the active cumulus effects calculation. Some of the interstitial aerosol is then transferred to the convective-cloud-borne state, in order to provide an initial chemical composition of the cloud water. For this, we assume that the cloud-borne fraction for each aerosol chemical component (and size bin) is the same as the cloud-borne fraction in the steady-state updraft of the active cumulus. This is conceptually consistent with the passive clouds being decaying remnants of active clouds. Aqueous-phase chemistry calculations are then made for this passive cloud fraction, again over the lifetime of the cumulus. Finally, the passive cumulus fraction of the grid cell is mixed with the remainder of the grid cell, and convective-cloud-borne aerosol is partially transferred to grid-resolved cloud-borne aerosol and partially resuspended to interstitial aerosol.

After the passive cloud calculations, the grid-cell mean mixing ratios of aerosols and trace gases reflect the effects of active and passive cumulus over the cloud lifetime. These mixing ratios are returned to the host code as the updated mixing ratios. In our simulations, a primary time step (for dynamics) of 15 s was used, and a chemistry time step (for most processes involving trace gases and aerosols) of 5 min was used. The sub-grid cumulus lifetimes, as defined within the cumulus parameterization, ranged from 30 to 60 min, and the cumulus effects on aerosols/gases are calculated once only when a cumulus is triggered in a grid column. On subsequent chemistry time steps, no more cumulus effect calculations are performed until a new cumulus is triggered in a column. An alternate approach would be to save the cumulus effect tendencies for aerosols and gases, and then apply them gradually over the cumulus lifetime, analogous to the approach used in the cumulus physics for temperature, moisture, and momentum. We chose this one-time update approach for aerosols and gases for simplicity and to reduce memory costs associated with storing the cumulus effect tendencies for the many aerosol and gas species. The net changes to the aerosol would be the same in either case because of the steady-state assumption used for the cloud properties over the cumulus lifetime, but the changes are applied somewhat sooner in the once-only approach (when a cloud triggers rather than over its lifetime), producing small differences in a simulation that could grow over time.

## 3 WRF-Chem configuration

### 3.1 Experiment setup

WRF-Chem version 3.2.1 was configured in a way similar to that described by Shrivastava et al. (2013). A single domain, 2240 km on a side, over the central United States, was used with 10 km horizontal grid spacing. WRF-Chem was also configured to use 64 vertical levels, with approximately 25 levels in the lowest 1 km of the atmosphere. The various parameterizations utilized in the simulations, not including the modifications described in Sect. 2, are listed in Table 1. Multi-day WRF-Chem simulations for the period of 1 June through 30 June 2007 were completed in individual 36 h blocks. The first 12 h of each block were discarded and the final 24 h saved for analysis. Meteorological initial and boundary conditions for each block were taken from the Global Forecast System (GFS). Boundary conditions of trace gases and aerosols were derived from the MOZART global simulation (Emmons et al., 2010b). Initial conditions for trace gases and aerosol were taken from the end of the previous simulation block.

Care must be taken when applying cumulus parameterizations in simulations that use an intermediate grid spacing where the sub-grid-scale motions can be nearly the same size as the model grid size (Wyngaard, 2004) and for cases in which the assumption is that the updraft area in the model grid box is small (Arakawa et al., 2011). Alternative approaches are being developed that include new scale-aware parameterizations (e.g., Gustafson et al., 2013; Grell and Freitas, 2014). In this study, the fraction of the model grid box occupied by cumulus convective updrafts was analyzed and was found to generally be less than 10 % (Fig. 2). The application of the cumulus parameterization at 10 km horizontal grid spacing used in this study is consistent with other work that has appeared in the literature (e.g., Larson et al., 2012; Berg et al., 2013), including Gerard et al. (2009), who identified horizontal grid spacing ranging from 2 to 7 km as prob-

lematic, and with recommendations made in the WRF Users Guide (Skamarock et al., 2008).

Three sets of simulations are used to investigate the regional impacts of cloud–aerosol interactions associated with both shallow and deep convection (Table 2). In all three simulations, the shallow and deep cumulus physics are enabled as well as aerosol processes (activation/resuspension, aqueous chemistry, and removal) in grid-resolved clouds. However, the cumulus effects on aerosols and trace gases are selectively enabled in the different simulations. The first simulation includes aerosol processing associated with both shallow and deep clouds, and is referred to as DeepShallow. This simulation can be used to estimate the regional impact on aerosol properties due to cloud processing associated with all clouds in the domain (including both grid-resolved and parameterized clouds). The second simulation has aerosol processing by shallow convection turned on and that by deep convection turned off, and is referred to as ShallowOnly. The difference between DeepShallow and ShallowOnly is used to document the impact of aerosol processing by deep convection alone and is identified as the Deep effect in this work. The third simulation is conducted with all aerosol processing by sub-grid convective clouds turned off (Control) and is the default treatment in WRF-Chem. The difference between ShallowOnly and Control simulations shows the impact of sub-grid shallow clouds and will be identified as the Shallow effect in the rest of the manuscript. An additional simulation was completed for a subset of the study period to document the impact of aqueous-phase cloud chemistry on aerosol composition. This was accomplished by repeating the DeepShallow simulation for 25 June 2007 with the convective cloud aqueous chemistry turned off. This run was initialized using the aerosol from the end of the previous DeepShallow simulation block.

### 3.2 Emissions

Hourly emissions used in this study are the same as those used by Shrivastava et al. (2013). In brief, hourly emissions of aerosol and trace gases are derived for the desired 2007 period by assuming a linear variation in the US Environmental Protection Agency's National Emissions Inventory (NEI; e.g., http://www.epa.gov/ttn/chief/net/2005inventory.html) for 2005 and 2008, supplemented with biomass burning gas and aerosol emissions taken from the 2007 Fire Inventory produced by NCAR (FINN07) (Wiedinmyer et al., 2011). The NEI contains two sizes of particulate matter emissions: particles with diameters less than or equal to 2.5 µm ($PM_{2.5}$) and those less than or equal to 10 µm ($PM_{10}$). NEI $PM_{2.5}$ emissions are divided into categories of sulfate, nitrate, organic aerosol, elemental carbon, and unspeciated primary $PM_{2.5}$, following Hsu et al. (2006). As in Shrivastava et al. (2013), all unspeciated $PM_{2.5}$ is lumped into the MOSAIC other inorganic material (OIN) category. For the simulations presented here, OIN accounts for approximately

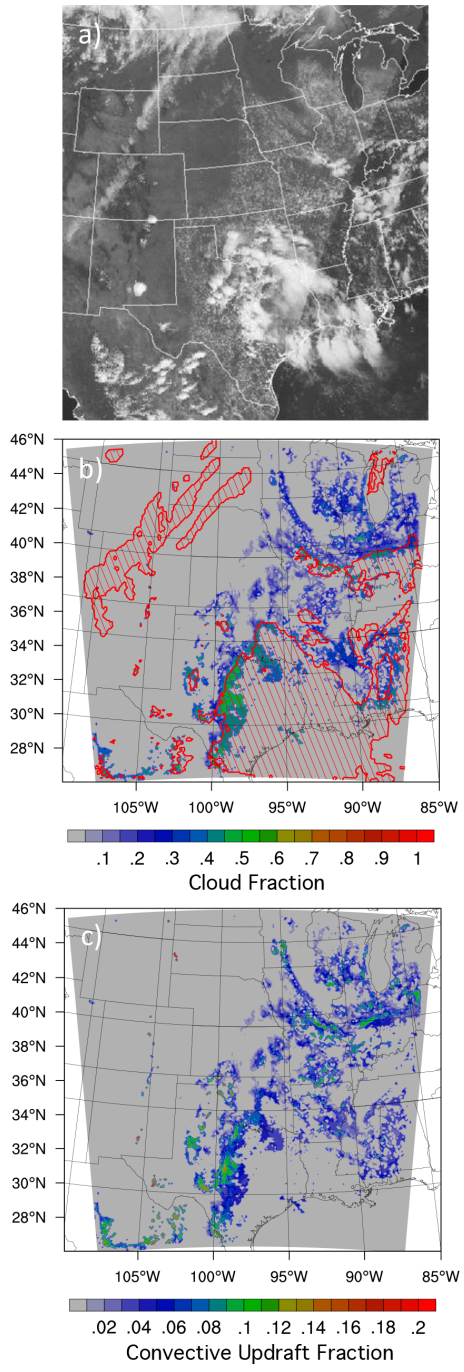


**Figure 2.** GOES visible satellite image valid at 20:15 UTC, 25 June 2007 **(a)**, and simulated cloud fraction associated with the KF–CuP parameterization (colors), areas with grid-resolved clouds (hashed; **b**), and fraction of model grid box with convective updrafts **(c)**. Note the different color scales used in plots of cloud fraction **(b)** and convective updraft fraction **(c)**.

77 % of the $PM_{2.5}$ mass emissions. The MOZART model (Emmons et al., 2010a) was used to provide the inflow of dust through the boundaries of the WRF-Chem domain, with these values assumed to be OIN. $PM_{2.5}$ and $PM_{10}$ emissions

**Table 1.** WRF-Chem configuration used in this study.

| Physical process | Parameterization |
|---|---|
| Surface | Noah land-surface model (Chen et al., 1996) |
| Boundary layer | Mellor–Yamada–Janjić (Janjić, 1990, 2002) |
| Cloud microphysics | Morrison two-moment (Morrison et al., 2005, 2009) |
| Cumulus | Kain–Frisch (with CuP modifications) (Kain and Fritsch, 1990; Kain, 2004; Berg et al., 2013) |
| Radiation (shortwave and longwave) | CAM 3 (Collins et al., 2004) |
| Gas-phase chemistry | SAPRC-99 (Carter, 2010) |
| Aqueous chemistry | Fahey and Pandis (Fahey and Pandis, 2001; Chapman et al., 2009). |
| Aerosol chemistry | MOSAIC for inorganic aerosols (Zaveri et al., 2008); simplified volatility basis set (VBS) for organic aerosol (Shrivastava et al., 2011). Eight size bins, dry diameters 0.039–10 μm. |

**Table 2.** Definitions of simulations completed as part of the study. The parameterized cumulus dynamics are applied in all simulations.

| Simulation | Aerosol processing by shallow and deep cu | Status (on/off) |
|---|---|---|
| DeepShallow | Aerosol processing shallow cu | On |
| | Aerosol processing deep cu | On |
| ShallowOnly | Aerosol processing shallow cu | On |
| | Aerosol processing deep cu | Off |
| Control | Aerosol processing shallow cu | Off |
| | Aerosol processing deep cu | Off |

are mapped to eight size bins for the sectional size distribution representation following Fast et al. (2006). Particles in each size bin are assumed to be internally mixed and the same size distribution is assumed for all species. VOC emissions were speciated using the SAPRC-99 mechanism and biogenic VOC emissions are estimated using the Model of Emissions of Gases and Aerosols from Nature (MEGAN, http://bai.acd.ucar.edu) (Guenther et al., 2006). The 138 biogenic species in MEGAN are grouped into three classes for use with WRF-Chem. Primary emissions are further modified to account for semi-volatile and intermediate volatility organic compounds (S/IVOC) that are large potential anthropogenic SOA precursors and are co-emitted with primary organic aerosols (POAs) (Shrivastava et al., 2008). In this study, emissions of SVOC are assumed to be twice those of POAs for anthropogenic sources, while IVOC emissions are estimated to be 1.5 times the sum of SVOC and POA emissions, for total S/IVOC emissions equal to 6.5 times POA (Hodzic et al., 2010; Tsimpidi et al., 2010; Shrivastava et al., 2011). A two-species volatility basis set (VBS) mechanism is used here, with both POA and secondary organic aerosols (SOA) assumed to have a very low volatility (Shrivastava et al., 2011). In previous work, Shrivastava et al. (2013) showed that this two-species VBS mechanism resulted in reasonable predictions of organic aerosols compared to measurements made during CHAPS, as described in the next section.

## 4 Data

In this study, a subset of model results is compared to data collected during CHAPS, which was conducted during June 2007 and included the deployment of the Department of Energy's Gulfstream-1 (G-1) aircraft and the National Aeronautics and Space Administration (NASA) Langley Research Center B200 aircraft. During CHAPS, the G-1 was configured for in situ sampling of aerosol chemical and optical properties (Berg et al., 2009). The flight path was specifically designed to measure conditions below, within, and above a population of shallow cumuli near Oklahoma City, Oklahoma. The size distribution of aerosol and cloud droplets was measured using a Droplet Measurement Technologies (DMT) passive cavity aerosol spectrometer probe (PCASP) and a DMT cloud aerosol spectrometer (CAS). The G-1 was equipped with two aerosol inlets: an isokinetic inlet for sampling aerosol in clear air and interstitial aerosol within clouds, and a counter flow virtual impactor (CVI) to sample only cloud droplets. An Aerodyne aerosol mass spectrometer (AMS) was used to analyze the composition of non-refractory aerosol sampled via both inlets. In their work, Shrivastava et al. (2013) evaluated the performance of WRF-Chem for the same period and found reasonable agreement with the observations when the model was run with relatively fine spatial resolution (2 km) that explicitly represented convection. They reported some discrepancies between the simulated and observed aerosol optical properties, but these were attributed to assumptions related to the emissions, hygroscopicity, and complex index of refraction of OIN particles, in addition to aerosol water content.

The B200 was equipped with the downward looking NASA Langley high spectral resolution lidar (HSRL-1) that provided height-resolved observations of aerosol backscatter,

extinction, and depolarization that were nearly simultaneous with the in situ G-1 measurements. Details of the HSRL-1 system can be found in Hair et al. (2008). The HSRL-1 uses the spectral distribution of the lidar return signal to separate the molecular and aerosol signals and can independently determine the aerosol backscatter, extinction, and depolarization at a wavelength of 532 nm. The HSRL-1 also functions as a standard backscatter lidar at a wavelength of 1064 nm, measuring both backscatter and depolarization at that wavelength. During CHAPS, the B200 aircraft flew above the G-1, providing lidar "curtains" along the flight track.

## 5 Analysis

In a previous case study, Berg et al. (2013) showed that the use of the KF–CuP parameterization in WRF led to a significant increase in the number of simulated shallow sub-grid convective clouds for 3 days in 2007 (16 May, 2 July, and 24 July) over the Department of Energy's Atmospheric Radiation Measurement (ARM) Central Facility, consistent with observations. In contrast, the standard KF scheme did a poor job representing the shallow clouds in these cases. Therefore, the performance of the cumulus parameterization will not be rigorously evaluated here. A single example of the model's ability to simulate the observed cloud fields is illustrated in Fig. 2, which shows the GOES visible image (valid at 20:15 UTC) and the cloud fraction associated with sub-grid clouds simulated by the cumulus parameterization and areas with grid-resolved clouds at 20:00 UTC on 25 June 2007. The KF–CuP parameterization predicts large areas with shallow convection over much of the central United States, which is consistent with the areas of shallow cumuli seen in the satellite image over much of Iowa, Kansas and Missouri, and a number of deep convective clouds over Texas and Oklahoma. The frequency of occurrence in which shallow or deep convection was triggered in the WRF grid columns for the period 12:00–20:00 UTC on 25 June 2007 is shown in Fig. 3 and provides information about the air-mass history in regards to sub-grid cumuli within the three boxes. Note that there can be cases in which the color shading indicates both shallow and deep clouds in the same model grid column. This occurs when different cloud types occur at different times of the day.

Due to the spatial inhomogeneity of the cloud fields over the central United States highlighted in Fig. 2, our analysis of conditions on 25 June will focus on three different distinct regions each approximately 240 km to a side, not just the CHAPS area around Oklahoma City that was analyzed by Shrivastava et al. (2013). These areas, approximately centered on Madison, Wisconsin (MSN), Austin, Texas (AUS), and Oklahoma City, Oklahoma (OKC), were selected because they contain primarily shallow convection (MSN), deep convection (AUS), or a mixture of both (OKC) (see Fig. 3), and allow us to better understand the behavior

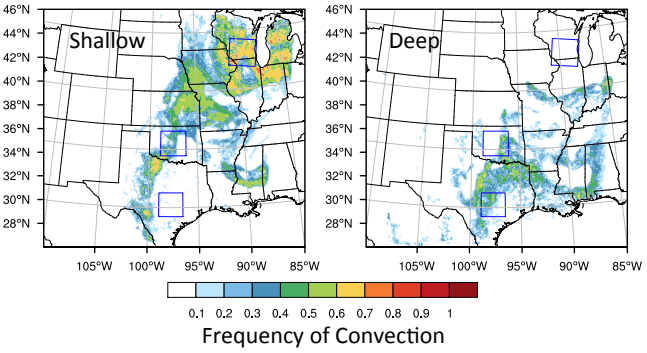


**Figure 3.** Frequency of occurrence of deep convection (right) and shallow convection (left) for the time period 12:00–20:00 UTC on 25 June 2007. Boxes indicate sub-regions, 240 km on a side, selected for analysis.

of the model and its parameterizations over a range of conditions. The MSN box has a very high frequency of shallow clouds distributed over the box, with the nearest upstream deep convection occurring over central Illinois. The AUS box has a very low frequency of simulated sub-grid shallow clouds and a much higher frequency of simulated sub-grid deep convective clouds. In contrast to the other two boxes, the OKC box includes a mixture of both shallow and deep convection.

While MOSAIC represents multiple aerosol constituents, only BC, OA, and sulfate have been selected for analysis within the three boxes. These particular constituents were selected because of their climatic relevance, and their representative behavior. BC is, to a first approximation, only impacted by transport, activation/resuspension, dry deposition, and wet removal – and in the case of non-precipitating convection, acts essentially as a passive tracer. Although freshly emitted BC is hydrophobic, the internal mixing assumption applied in the model causes it to quickly reside in hygroscopic particles. Interpretation of cloud–aerosol interactions and vertical sulfate transport is more complicated than for BC because sulfate can be produced within cloud droplets via aqueous-phase oxidation of dissolved sulfur dioxide gas as well as removed via precipitation (e.g., Easter and Hobbs, 1974; Hegg et al., 1986; Tremblay and Leighton, 1986; Chaumerliac et al., 1987; Taylor, 1989; Wang and Chang, 1993; Koch et al., 2003). While the majority of OA in the atmosphere is secondary and is somewhat hygroscopic, its behavior within convective clouds is similar to that of BC aerosol because the aqueous chemistry related to OA production is not fully understood and currently is not included in the model.

### 5.1 Local impacts on aerosol vertical distribution

One important impact of convective clouds is the vertical redistribution of aerosol due to the impact of convective updrafts, downdrafts, entrainment mixing, enhanced subsi-

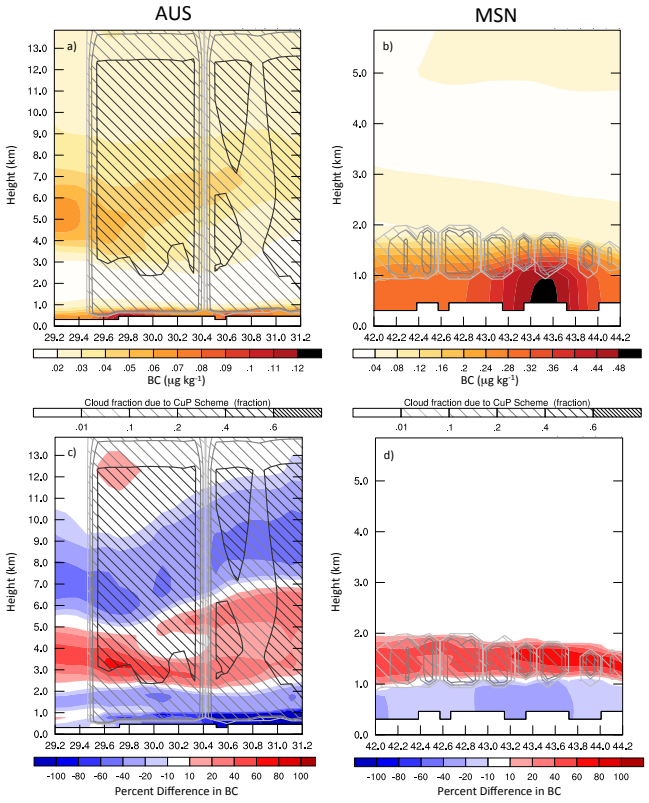


**Figure 4.** Vertical north–south cross sections of the BC mixing ratio summed over size bins 1 through 4 (color shading in **a, b**; μg kg$^{-1}$), including both interstitial and activated aerosol in the cloudy grid cells, and the difference in the BC mixing ratio between DeepShallow and Control simulations (color shading in **c, d**; percentage) for conditions dominated by deep convective cloud (AUS; **a, c**) and shallow convective cloud (MSN; **b, d**) boxes at 20:00 UTC on 25 June 2007. Hatching indicates the cloud fraction associated with sub-grid convective clouds. The horizontal axes are labeled in degrees of latitude and the vertical axes are the height above mean sea level.

dence, and wet removal associated with sub-grid clouds. Figure 4 shows examples of vertical north–south cross sections (through the center of the analysis boxes) of the amount of BC (including both interstitial and activated aerosol in the cloudy grid cells) for the DeepShallow case and the fractional change in BC loading between the DeepShallow and Control simulations (indicated by the colors) as well as the cloud fraction (indicated by the gray shading) within the AUS and MSN boxes valid at 20:00 UTC on 25 July 2007. Within both the AUS and MSN boxes, the largest BC mass loadings are found near the surface. There are also large amounts of BC 4–6 km above the surface in the AUS cross section that is apparent in both the DeepShallow (Fig. 4) and Control simulations (not shown). This elevated layer is not associated with convection, but rather with long-range transport, most likely from a fire located in central New Mexico (not shown) and a coal-fired power plant in Colorado.

At first glance it might be surprising that there are no columns of enhanced aerosol loading within the AUS clouds due to enhanced upward transport from the sub-cloud layer shown in Fig. 4. Their absence is primarily due to the wet removal of aerosol within the lowest levels of the clouds, as well as the cloud fraction (which ranges from 20 to 60 % within the deep convective clouds shown in the figure), which reduces the relative impact of the aerosol in the updraft, within any given model grid cell. In the AUS cross section, the large fractional increase in BC between the DeepShallow and Control simulations for altitudes ranging from 3 and 5 km and the decrease above 5 km can be attributed to vertical transport by updrafts, downdrafts, and convection-induced subsidence. At these altitudes (which are below the detrainment level), this transport replaces some of the air (and aerosol) in a grid cell with air from higher levels that has smaller BC concentrations.

Within the AUS cross section, the clouds extend from an altitude of approximately 0.5 to nearly 15 km. The clouds in the MSN box are much shallower, extending from approximately 1 to 2 km, as is more typical for boundary-layer cumuli (e.g., Berg and Kassianov, 2008). The decrease in the amount of BC loading in the sub-cloud layer is caused by the venting of aerosol out of that layer by the convective clouds. In contrast to the AUS box that includes deep sub-grid convective clouds, the vertical extent of the transport of BC is more limited within the MSN box (Fig. 4b). This result is consistent with the much smaller vertical extent of the clouds in this box. Within the cloud layer, the shallow cumuli still have an important impact on the vertical extent of the BC (Fig. 4d). The fractional difference in the BC between the DeepShallow and Control simulations approaches 50 % as the convective clouds transport BC from below the cloud into the cloud layer. The net effect of the non-precipitating cumuli is to mix BC over the sub-cloud and cloud layers, which is consistent with the findings of others (e.g., Vilà-Guerau de Arellano et al., 2005; Kim et al., 2012).

Similar to the case for BC, there is an elevated plume of sulfate aerosol near an altitude of 5 km in the AUS cross section that is associated with long-range transport (Fig. 5a). In both the AUS and MSN cross sections, there is a large concentration of sulfate within the boundary layer that is associated with surface emissions. As with BC, fractional differences between the DeepShallow and Control runs are much larger than 50 %. Within the AUS box, there is a large fractional change in the amount of sulfate aloft that can be attributed to vertical transport by updrafts, downdrafts, and convection-induced subsidence that are represented in the DeepShallow simulations (Fig. 5c). The situation is different in the MSN box, where all of the clouds are shallow non-precipitating cumuli (Fig. 5b, d). In this case, the vertical transport is limited to the cloud layer (altitudes lower than approximately 2 km), where there is significant increase in the sulfate loading in the cloud layer (Fig. 5b). In contrast to the BC within the MSN box, the sulfate is enhanced in the

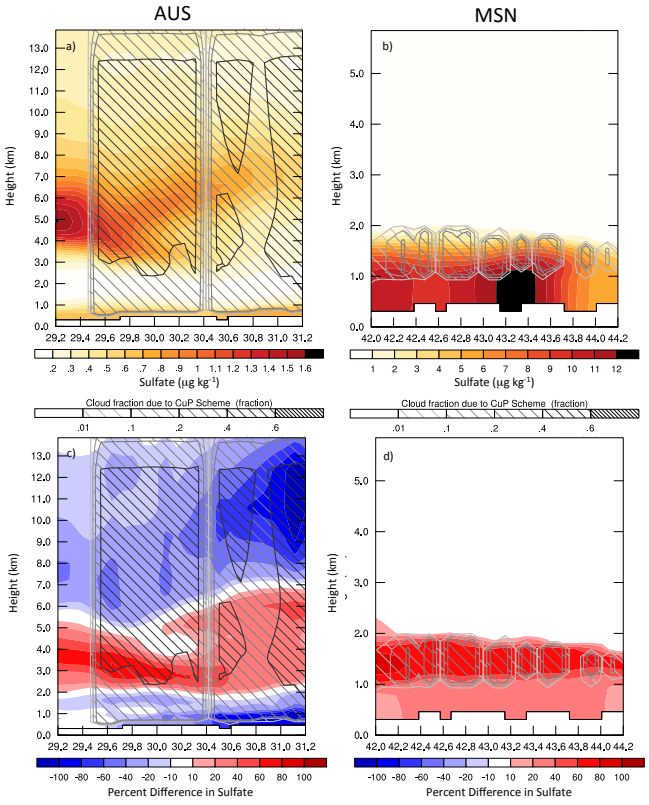


**Figure 5.** Same as Fig. 4 but for sulfate.

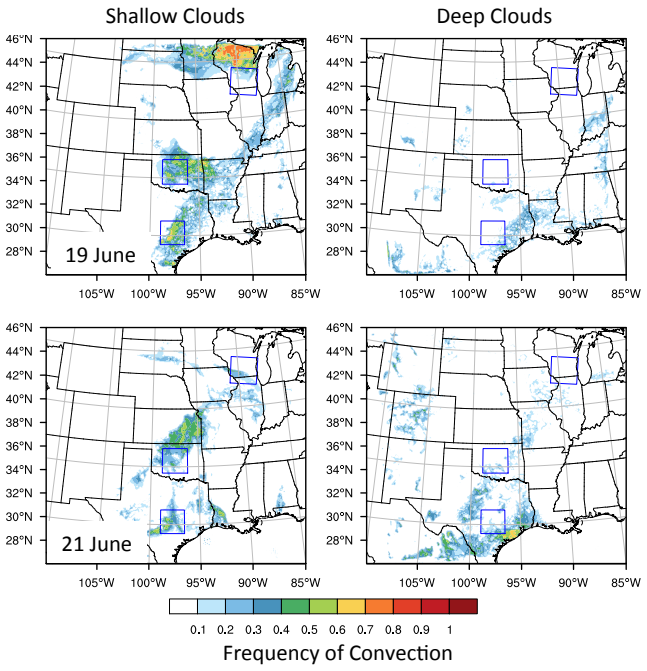


**Figure 6.** Frequency of occurrence of deep convection (right) and shallow convection (left) for the time period 12:00–20:00 UTC on 19 (top) and 21 June (bottom) 2007.

ShallowOnly simulations both below and within the cloud layer. This is due to sulfate production within clouds, the detrainment of cloudy air with enhanced sulfate, and subsequent downward transport of air back into the subcloud layer. There is no evidence of lofted sulfate in the levels above the shallow cumuli (Fig. 5b).

Using data from the G-1 aircraft alone, it is difficult to verify the simulation of the vertical transport of aerosol associated with cumulus. Data from the airborne NASA HSRL, however, can be used to investigate the vertical extent of aerosol in the vicinity of convective clouds. This data set does not provide information in regards to the speciation of the aerosol, but it can be used to look at impacts on the aerosol backscatter and extinction, which are highly correlated with the aerosol loading. Unfortunately, HSRL data are not available for 25 June, so 2 other days have been selected for analysis of vertical transport, including 19 and 21 June 2007. The frequency of simulated shallow and deep clouds is shown in Fig. 6, and both days had relatively large numbers of simulated shallow clouds both before and during the G-1 and B200 flights.

Conditions on 19 June were marked by large numbers of both observed and simulated shallow cumuli near Oklahoma City and are similar to the MSN grid box on 25 June. In most cases, the observed shallow cumuli are sufficiently optically thick so that the laser beam is attenuated by the cloud, leading to the frequent periods of missing data below the cloud top (as indicated by the white areas underneath peaks in the aerosol backscatter in Fig. 7). On 19 June, the majority of cloud-top heights measured by the HSRL are found to range from 1 to 2.5 km and there are relatively large amounts of aerosol backscatter and extinction from the surface to an altitude of 2.5 km, which roughly corresponds to the highest cloud-top heights observed during the B200 flight. The DeepShallow and Control simulations were subsampled along the B200 flight track and the fractional difference in the WRF-Chem simulated extinction and the cloud fraction associated with convective clouds is shown in Fig. 7c. Both the DeepShallow and Control simulations underestimate the aerosol extinction on 19 June by a factor of approximately 1.25 to 2.0 compared to the values derived from the HSRL (not shown). This is likely due to both an underestimate of aerosol mass loading as well as an underestimate of the simulated water uptake by the aerosol. Given that both sets of simulations underestimate the observed values, the underestimate of backscatter and extinction is not attributable to the treatment of sub-grid convective clouds. The simulated cloud fraction reaches values as large as 40 % and the vertical extent of the simulated clouds is consistent with the HSRL observations. The largest positive differences in the simulated extinction are associated with the layer of shallow cumuli. The enhanced transport associated with the DeepShallow simulations spread the aerosol, and hence aerosol extinction, over a layer from the surface to an

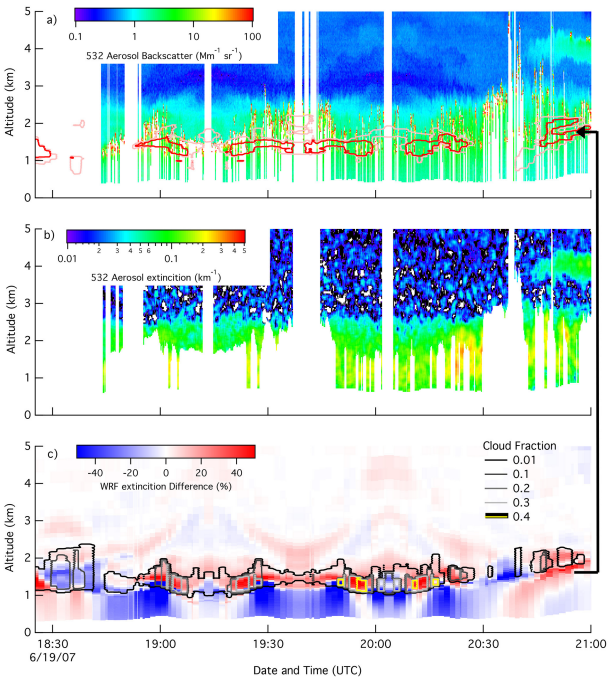


**Figure 7.** Cross sections of observed aerosol backscatter **(a)**, aerosol extinction **(b)** at a wavelength of 532 nm, and the difference in aerosol extinction of DeepShallow and Control simulations **(c)** on 19 June 2007. Contours in **(a)** mark contours of +10 and +20 % difference in the WRF-Chem simulations, as indicated by the large arrow, and contours in **(c)** indicate simulated cloud fraction as indicated by the legend.

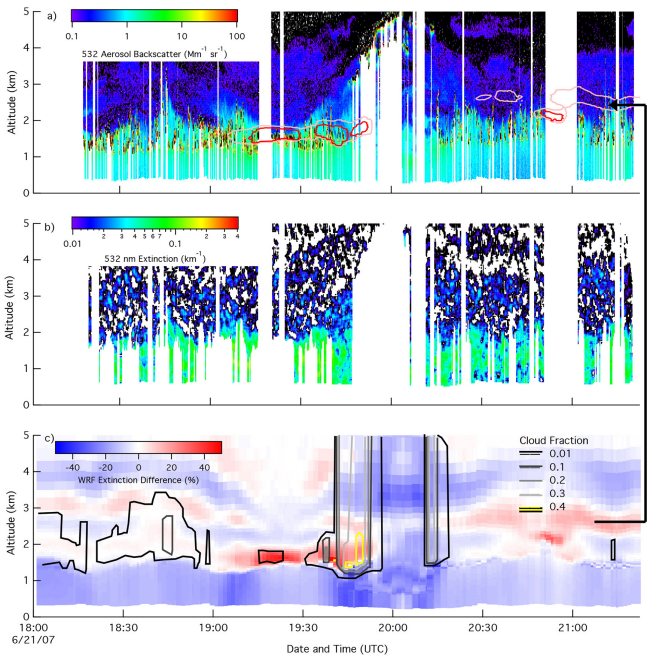


**Figure 8.** Same as Fig. 7 but for 21 June 2007.

altitude of 2 km, compared to only 1 km in the Control simulations. The values of extinction in the DeepShallow simulations are 10–20 % greater over altitudes ranging from 1 to 2 km than was found in the Control simulations, while the extinction in the subcloud layer is reduced by a similar magnitude. This behavior is similar to the changes seen with the BC loading within the MSN analysis box on 25 June (Fig. 4). The differences between the DeepShallow and ShallowOnly simulations are subtle on 19 June (not shown), because of the relatively small amount of deep convection in the vicinity of the OKC analysis box. There is, however, still a decrease in the aerosol mass loading in the DeepShallow simulations compared to the ShallowOnly case.

In contrast to 19 June, which had a large fraction of shallow convection and very few deep clouds near Oklahoma City, conditions on 21 June were marked by a mixture of deep and shallow clouds in both the observations and simulations. The HSRL data show a region of higher clouds (near 20:00 UTC; Fig. 8). The tops of the observed shallow clouds range from approximately 1 to 2 km and are distributed along much of the entire flight track. The vertical transport associated with the clouds leads to enhanced aerosol backscatter and extinction to an altitude of 2 km. There are fewer simulated clouds along the flight track at the time of the B200 flights than is observed, and there are some simulated deep convective clouds between 19:30 and 20:00 and near 21:15 UTC (Fig. 8). There are some systematic changes in the simulated aerosol extinction, suggesting additional clouds upwind of the flight track, or clouds that occur before the B200 was aloft. These changes include an increase in the aerosol extinction in the DeepShallow simulations near an altitude of 1.75 km between 19:00 and nearly 20:00 UTC, and near an altitude of 2 km from 20:15 through approximately 21:30 UTC. The results for 21 June are reminiscent of changes seen in the AUS analysis box for 25 June and suggest an increased impact of deep convection on 21 June than was seen on 19 June.

There are differences between the results of the DeepShallow simulation shown in Fig. 8 and the ShallowOnly simulation (not shown) that demonstrate the relative importance of the deep clouds. The ShallowOnly simulation has more extinction for altitudes higher than 1.5 km, which is associated with less wet removal and less vertical transport. This is particularly the case around 20:30 UTC, where the DeepShallow simulation has a large decrease in extinction associated with the deep clouds (Fig. 8). While there are no deep convective clouds shown in the lidar cross section (there were some clouds with tops as high as 5 km), it is difficult to evaluate the relative skill of the parameterization to predict the occurrence of deep convective clouds from a single cross section. It should be noted that, on this particular day, there were a number of both simulated and observed deep clouds near the sampling domain.

### 5.2 Regional-scale impacts

The results presented in Sect. 5.1 highlight the fact that the parameterization is performing reasonably and can be used to investigate the regional impacts of cloud–aerosol interactions within the areas defined by the analysis boxes. The primary advantage of using a parameterization to represent convective clouds is the ability to run simulations over a large domain, which enables the evaluation of regional-scale impacts of cloud–aerosol interactions on the aerosol life cycle that is not possible using high-resolution simulations. Differences in the column-integrated mass loading are one method that can be used to investigate changes in mass loading of atmospheric aerosol over large areas. BC represents particles that are essentially passive tracers (ignoring wet and dry removal) that do not undergo aqueous-phase chemistry in simulated clouds. Overall, there is a significant reduction in the column-integrated BC and OA across the model domain (Fig. 9). The primary removal mechanism added in the DeepShallow simulations (compared to the Control simulations) is the wet removal associated with the parameterized precipitation. This leads to systematic decreases of as much as $-50$ % in the amount of BC. It is interesting to note that there is a net decrease in BC within the MSN box in which there is no convection and very little grid-resolved precipitation, indicative of wet removal upwind of the box during the simulation and pointing to regional-scale impacts of cloud–aerosol interactions. There are also small areas in which the column-integrated BC loading is larger in the DeepShallow simulations than in the Control simulations. These features are also present in the ShallowOnly case (not shown). The increase in the column-integrated BC in the AUS box is the result of slight differences in the path of the aerosol plume coming from the Houston, Texas, area. Different aerosol loadings in the simulations produce different feedbacks on meteorology (i.e., aerosol indirect effects in grid-resolved clouds and aerosol direct effects), leading to small differences in winds. In the DeepShallow simulations, the main part of the plume is shifted a small distance to the north, giving rise to the apparent increase in the BC loading just downwind of Houston.

The OA follows a pattern similar to what is seen for BC, but the fractional change is smaller in magnitude. Currently in WRF-Chem the OA are unaffected by aqueous chemistry within the clouds, but can be affected by changes in the amount of precursor gases. Vertical transport of SOA precursor gases (which are not wet-removed in our parameterization) to higher and colder altitudes can result in more partitioning to the particle phase. These changes lead to areas, such as the central swath through the OKC box, and over parts of the southeastern United States, where there is an increase in the column-integrated OA. Based on these simulations, the change in OA can be significant, approaching a column-integrated increase of 10 to 15 % for some areas.

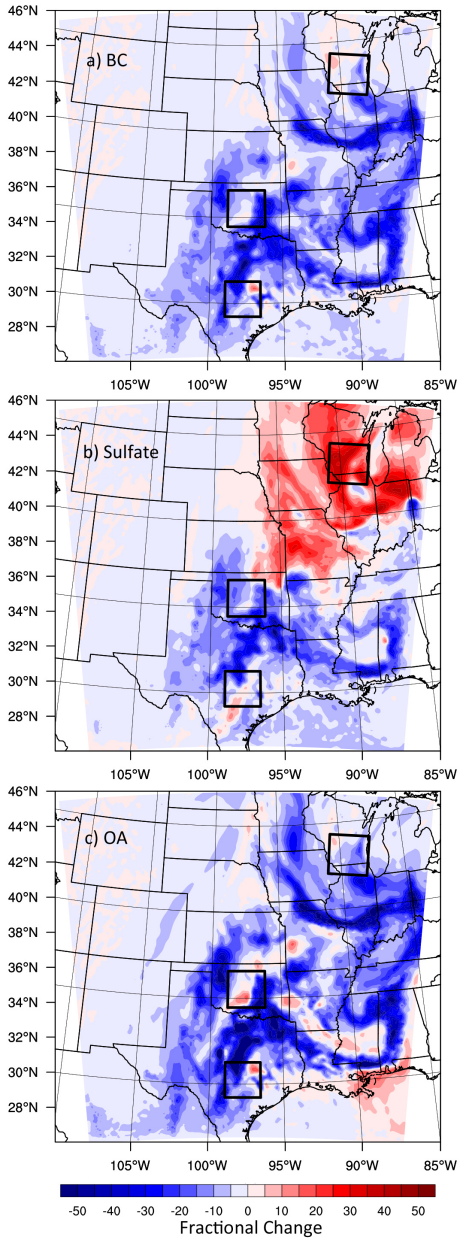


**Figure 9.** Fractional differences in column-integrated aerosol mass loading between DeepShallow and Control simulations for size bins 1 through 4, including both interstitial and activated aerosol in the cloudy grid cells, for BC **(a)**, sulfate **(b)** and OA **(c)**, valid at 20:00 UTC on 25 June 2007. Black boxes indicate boxes used in the analysis.

In contrast to BC, the wet removal of sulfate can be counteracted by its production in cloud. In the AUS box, sulfate wet removal is larger than production, leading to a small net decrease in sulfate when cloud–aerosol interactions (including aqueous chemistry) associated with deep and shallow clouds are considered. Within the MSN box (and over much of the upper Midwest), there is no convective and very little

grid-resolved precipitation, so that the production of sulfate aerosol by aqueous chemistry dominates and there is a significant increase in the column burden of sulfate when non-precipitating clouds are present (Fig. 9). The additional sulfate is limited to the cloud layer and below, but, as shown in Fig. 5, this enhanced sulfate can spread over a deeper layer of the atmosphere. Relative to the Control case, where the impacts of cumulus are ignored, our results indicate that cumulus can increase the column sulfate burden by as much as 40 %. While the simulations shown here were rather short, longer integration times could lead to significant differences downwind of the area of sulfate production due to enhanced vertical mixing and regional-scale transport.

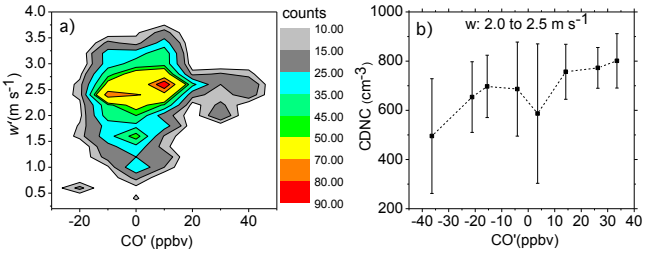


**Figure 10.** PDF of simulated cloud updraft speed and CO loading in cloudy updrafts **(a)**, and change in CDNC with perturbation values of CO (CO') for perturbation values of $w$ ($w$') between 2.0 and 2.5 m s$^{-1}$ **(b)**. Error bars in **(b)** indicate the standard deviation.

### 5.3 Impact on cloud microphysics

Using data collected during CHAPS, Berg et al. (2011) measured differences in cloud microphysical properties that could be explained by differences in the aerosol concentrations and vertical velocities within individual clouds. They used the carbon monoxide mixing ratio perturbation (CO', defined as the difference between the instantaneous measured CO and the average CO observed during a flight leg) as an indicator of increased aerosol. They found systematic increases in the cloud droplet number concentration (CDNC) associated with both increases in CO' and the cloud updraft strength, which highlighted the importance of considering both the aerosol loading and the cloud dynamics. In their analysis of high-resolution WRF-Chem simulations, Shrivastava et al. (2013) found results consistent with those reported by Berg et al. (2011). A similar analysis has been completed here using results from the DeepShallow simulations in the OKC analysis box, but limited to only grid columns with shallow convection. The cloud microphysical properties were computed for only the cloudy updrafts, as this is the part of the parameterized clouds where the sub-cloud particle loading can influence the cloud microphysical properties via drop activation. A probability density function (PDF) of simulated CO' and perturbation vertical velocity ($w$', defined in a way analogous to CO') is shown in Fig. 10. In this case, the parameterized updraft speeds were found to range from 1.0 to 3.5 m s$^{-1}$, which are consistent with the updraft speeds in Fig. 1 of Berg et al. (2011).

For the parameterized sub-grid convective clouds, the CDNC is found to increase with increasing values of CO, showing an increase from about 500 to 800 cm$^{-3}$ (an increase by a factor of about 1.6) as the CO' ranges from clean (−35 ppbv) to dirty (+35 ppbv) for model grid cells where the updraft ranges from 2.0 to 2.5 m s$^{-1}$ (Fig. 10). The results are fairly noisy, with relatively large standard deviations highlighting the wide range of additional factors that can impact the CDNC. The slope of the CDNC vs. CO' regression lines for $w$' equal to 2.0–2.5 m s$^{-1}$ is computed to be 4.2 cm$^{-3}$ ppbv$^{-1}$, which is smaller than the 7.2 cm$^{-3}$ ppbv$^{-1}$ reported by Berg et al. (2011), but is close to the value of 4.5 cm$^{-3}$ ppbv$^{-1}$ derived from the results of Shrivastava et al. (2013). The different slopes seen in the observations, those reported by Shrivastava et al. (2013), and this study, could be related to the smoothing of emissions, which has been documented in the literature in regards to both simulated cloud characteristics (Gustafson et al., 2007) and aerosol loadings (Gustafson et al., 2011). The results shown by the different studies should be considered with care, however, because of the different vertical velocity ranges used in each case. While not ideal, the different $w$ ranges were applied because of differences in the spatial and temporal scales associated with the observations and high- and low-resolution simulations.

### 5.4 Chemical composition of cloud droplets

Changes to chemical properties of the particles associated with passage through clouds are an important aspect of cloud–aerosol interactions. One of the goals of the CHAPS study was to document changes in the chemical composition of particles that served as CCN (activated) or remained inactive (interstitial). During CHAPS, measurements showed that both the activated and interstitial aerosol were dominated by organics and sulfate (Fig. 11). In their analysis, Berg et al. (2009) also reported enhanced nitrate in the dried cloud droplet residuals that were sampled via a counter flow virtual impactor (CVI), consistent with model results presented by Hegg et al. (1986). They attributed this to the uptake of gas-phase nitric acid by cloud droplets. In their analysis of high-resolution WRF-Chem simulations, Shrivastava et al. (2013) also found enhanced nitrate when aqueous-phase chemistry, which includes trace gas–liquid phase equilibria, was turned on. When aqueous-phase chemistry was turned off in their simulations, however, the particle nitrate in cloud droplet residuals and interstitial particles was nearly the same, indicating the importance of the uptake and dissociation of gas-phase nitric acid within cloud droplets.

A similar analysis has been completed for the OKC box using results from ShallowOnly simulations. The mass loading of the interstitial aerosol within the shallow clouds is generally smaller in this study than the loading reported by

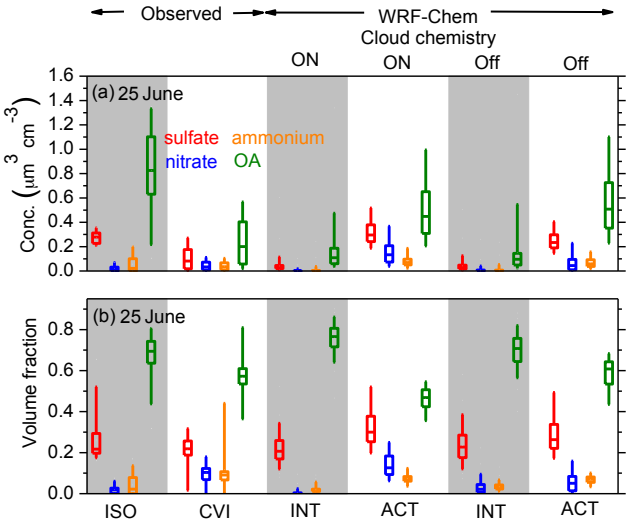


**Figure 11.** Aerosol mass concentration **(a)** and volume fraction **(b)** for observed interstitial (sampled via an isokinetic inlet (ISO; gray areas)) and activated (sampled via a counter-flow virtual impactor inlet (CVI; white areas)) aerosol; and simulated interstitial (INT; gray areas) and activated (ACT; white areas) aerosol at 20:00 UTC on 25 July 2007. Colors indicate sulfate (red), ammonium (orange), nitrate (blue), and organic aerosol (green) in size bins 1 through 4. Box-and-whisker plots indicate the 90th, 75th, 50th, 25th, and 10th percentiles.

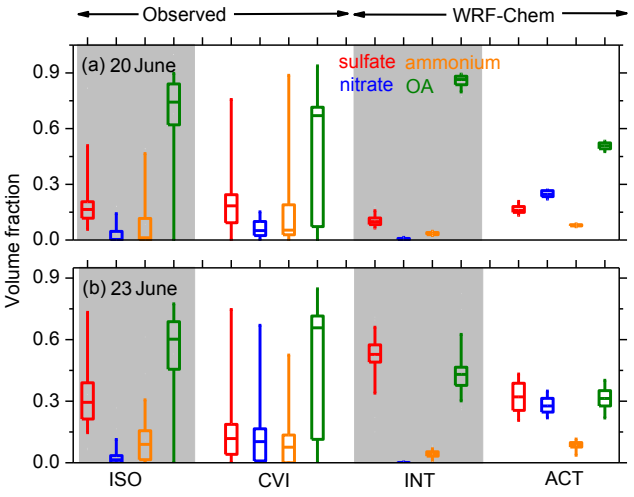


**Figure 12.** Similar to Fig. 11 but only for aerosol volume fraction on 20 **(a)** and 23 **(b)** June 2007. WRF-Chem results are only for cases in which the aqueous chemistry is turned on.

Shrivastava et al. (2013) for either the observations (Fig. 11) or high-resolution simulations (Fig. 7 of Shrivastava et al., 2013). This behavior may, in part, be attributed to the averaging of the emissions over the larger model grid cell in the vicinity of Oklahoma City and the location of the simulated shallow clouds in the two studies. In contrast to the interstitial particles, the simulated mass loading of the activated aerosol is larger in all three simulations (grid-resolved, ShallowOnly with cloud chemistry on, and ShallowOnly with cloud chemistry off) than the loading that was observed during CHAPS. The overestimation of simulated aerosol mass may, in part, be due to the cut size used by the CVI operated on the aircraft that would exclude small cloud droplets. In contrast to the aerosol mass loading, the observed and simulated aerosol volume fractions are in good agreement. Thus, even if the mass loading is incorrect, the consistent volume fractions indicate that the chemical processing within the model clouds is behaving in a way that is consistent with the observations. Similar to the observations and high-resolution simulations, there is an increase in the volume fraction of nitrate in activated (cloud-borne) aerosol compared to interstitial aerosol.

The analysis of activated versus interstitial aerosol composition is repeated for the CHAPS flights on 20 and 23 June. These days also had shallow cumuli in the vicinity of Oklahoma City, although the simulated cloud fraction (not shown) was less than that observed on 19, 21, and 25 June. On 20 June, the median organic volume fractions of interstitial aerosol were approximately 75 % organics and 15 % sulfate, with small amounts of nitrate and ammonium (Fig. 12a). The activated aerosol sampled using the CVI was also dominated by organics, but there was a great deal of variability in the volume fraction of organics as well as an increase in the volume fraction of nitrate. The ShallowOnly simulations for the OKC box for 20 June are consistent with the observed values and follow the same trends for both interstitial and activated aerosol. The variability in the simulated volume fraction is much less than was observed, which could be a result of the relatively small number of simulated sub-grid convective clouds on that day. The simulated activated aerosol also had enhanced values of nitrate aerosol compared to the interstitial aerosol. Observations on 23 June include a smaller volume fraction (60 %) of organics in the case of interstitial aerosol, and an increased volume fraction of sulfate (30 %) compared to the other 2 days (Figs. 11, 12b). The volume fraction of activated aerosol is also dominated by organics, but like conditions on 20 June, there is a great deal of variability. The ShallowOnly simulations have a relatively large median volume fraction associated with sulfate aerosol that is consistent with observations and smaller amounts of organic aerosol than were seen on 20 and 25 June. The simulations also have an enhanced nitrate volume fraction compared to the interstitial aerosol. Thus, the increase in nitrate aerosol seen in both the observations and simulations associated with aqueous chemistry is not limited to a single day, but rather is found to be a relatively common occurrence in the OKC box during CHAPS.

## 6 Summary and conclusions

A new treatment of cloud–aerosol interactions within parameterized shallow and deep convection has been implemented in WRF-Chem with the goal of improving regional-scale simulations of the aerosol life cycle and cloud–aerosol interactions. The modifications designed to represent cloud–aerosol interactions include treatment of the cloud droplet number mixing ratio; key cloud microphysical and macrophysical parameters (including the updraft fractional area, updraft and downdraft mass fluxes, and entrainment) averaged over the population of shallow clouds, or a single deep convective cloud; and vertical transport, activation/resuspension, aqueous chemistry, and wet removal of aerosol and trace gases in warm clouds. These changes have been implemented in the WRF-Chem chemistry package as well as the Kain–Fritsch cumulus parameterization (Kain and Fritsch, 1990; Kain, 2004), which has been modified to better represent shallow convective clouds (Berg et al., 2013). Results from simulations using WRF-Chem are compared with data from the CHAPS field experiment (Berg et al., 2009, 2011) as well as high-resolution simulations (Shrivastava et al., 2013).

The results are encouraging and demonstrate the advantages of the modifications that have been made to WRF-Chem. It is shown that both deep and shallow convective clouds have an important impact on the horizontal and vertical distribution of aerosol loading. Three different domain sub-regions were selected for detailed analysis, including locations near Madison, Wisconsin (MSN), Austin, Texas (AUS), and Oklahoma City, Oklahoma (OKC), the last corresponding to the site of CHAPS and the domain used in previous high-resolution simulations. These regions were selected to represent instances dominated by shallow (MSN), deep (AUS), or a mix of both (OKC) types of convective clouds. In each case, the WRF-Chem simulations behaved in a manner consistent with expectations and consistent with both the CHAPS data and the results of high-resolution simulations. In the case of shallow clouds, enhanced mixing leads to a deepening of the layer containing BC and decreased amounts of BC near the surface. Results are similar for OA, but the net impact was found to be smaller. In contrast to BC, sulfate aerosol was enhanced throughout the layer due to sulfate production within clouds. In the vicinity of AUS, the impact of shallow convective clouds is minimal. There was a decrease in BC, OA, and sulfate in the sub-cloud layer due to vertical transport associated with deep convective clouds. There were also significant changes in the aerosol loading aloft that were the result of the impacts of updrafts, downdrafts, entrainment mixing, enhanced subsidence, and wet removal associated with the sub-grid clouds. In the area near OKC, both the deep and shallow sub-grid convective clouds had a significant impact on the simulated aerosol loading. The shallow sub-grid clouds led to a decrease in aerosol in the sub-cloud layer and an increase in aerosol aloft. The parameterized deep-convective clouds led to decreases in the BC and OA over the lowest 2 km and sulfate over the lowest 3 km of the atmosphere.

One of the motivations for the development of the improved parameterization is to allow the investigation of regional- and synoptic-scale aerosol transport. In our case-study period, there is a significant reduction in the BC and OA over much of the central United States. The primary removal mechanism added in the new treatment is the wet removal associated with the parameterized precipitation. Thus, the differences in the aerosol loading highlight the importance of wet removal in the aerosol life cycle on the regional scale. In contrast to BC and OA, there are large regions in which there are increases in the column-integrated sulfate due to the production of sulfate and the absence of wet removal in nonprecipitating clouds.

The behavior of the modified version of WRF-Chem in regards to the cloud microphysical properties and chemical composition of aerosol is also investigated. The results show that the modified version of WRF-Chem is able to reproduce changes in the cloud droplet number concentration in a way that is consistent with both high-resolution simulations and observations from CHAPS. The CDNC associated with the parameterized clouds was found to be less sensitive to pollutant loading than was observed (Berg et al., 2011), but was similar to that reported by Shrivastava et al. (2013) in their high-resolution simulations. The chemical composition of the simulated cloud droplet residuals is compared to the composition measured with an AMS operated behind a CVI inlet during CHAPS. While there were differences in the simulated and observed mass loadings, the simulated and observed mass fractions were consistent, including the presence of enhanced amounts of nitrate in the cloud droplet residuals. WRF-Chem is also able to accurately represent the increase in nitrate found in the observed cloud droplet residuals. Overall, these findings provide evidence that the modified version of WRF-Chem is able to represent key features of the cloud–aerosol interactions in a realistic way. While the results presented here utilized WRF-Chem version 3.2.1, the code is being ported to the latest version of WRF-Chem, and we anticipate including these changes in a future public release of WRF-Chem.

*Acknowledgements.* This research was supported by the Office of Science of the US Department of Energy as part of the Atmospheric System Research (ASR) program. The Pacific Northwest National Laboratory is operated by Battelle Memorial Institute under contract DE-AC06-76RLO 1830. The funding for the B200 and HSRL operations came from the NASA Science Mission Directorate, the Department of Energy ASR program, and the NASA CALIPSO project. The authors would also like to thank the NASA Langley King Air B-200 and DOE G-1 flight crews for their outstanding work in supporting these flights and measurements. J. Ogren of NOAA and E. Andrews of the Cooperative Institute for Research in Environmental Sciences (CIRES) deployed the CVI

during CHAPS. Data from the AMS were collected by Y.-N. Lee of Brookhaven National Laboratory (BNL), M. L. Alexander of the Pacific Northwest National Laboratory and J. Jayne of Aerodyne. Size distribution data were provided by G. Senum of BNL. G. Grell (NOAA) and R. Leung (PNNL) provided feedback on various aspects of the manuscript. We also thank three anonymous reviewers for valuable feedback on the manuscript.

Edited by: T. Butler

## References

Abdul-Razzak, H. and Ghan, S. J.: A parameterization of aerosol activation 2. Multiple aerosol types, J. Geophys. Res., 105, 6837–6844, doi:10.1029/1999jd901161, 2000.

Ahmadov, R., McKeen, S. A., Robinson, A. L., Bahreini, R., Middlebrook, A. M., de Gouw, J. A., Meagher, J., Hsie, E. Y., Edgerton, E., Shaw, S., and Trainer, M.: A volatility basis set model for summertime secondary organic aerosols over the eastern United States in 2006, J. Geophys. Res., 117, D06301, doi:10.1029/2011jd016831, 2012.

Alapaty, K., Herwehe, J. A., Otte, T. L., Nolte, C. G., Bullock, O. R., Mallard, M. S., Kain, J. S., and Dudhia, J.: Introducing subgrid-scale cloud feedbacks to radiation for regional meteorological and climate modeling, Geophys. Res. Lett., 39, L24809, doi:10.1029/2012gl054031, 2012.

Arakawa, A., Jung, J.-H., and Wu, C.-M.: Toward unification of the multiscale modeling of the atmosphere, Atmos. Chem. Phys., 11, 3731–3742, doi:10.5194/acp-11-3731-2011, 2011.

Barahona, D. and Nenes, A.: Parameterization of cloud droplet formation in large-scale models: Including effects of entrainment, J. Geophys. Res., 112, D16206, doi:10.1029/2007jd008473, 2007.

Berg, L. K. and Kassianov, E. I.: Temporal Variability of Fair-Weather Cumulus Statistics at the ACRF SGP Site, J. Climate, 21, 3344–3358, doi:10.1175/2007jcli2266.1, 2008.

Berg, L. K. and Stull, R. B.: Parameterization of Joint Frequency Distributions of Potential Temperature and Water Vapor Mixing Ratio in the Daytime Convective Boundary Layer, J. Atmos. Sci., 61, 813–828, doi:10.1175/1520-0469(2004)061<0813:pojfdo>2.0.co;2, 2004.

Berg, L. K. and Stull, R. B.: A Simple Parameterization Coupling the Convective Daytime Boundary Layer and Fair-Weather Cumuli, J. Atmos. Sci., 62, 1976–1988, doi:10.1175/jas3437.1, 2005.

Berg, L. K., Berkowitz, C. M., Hubbe, J. M., Ogren, J. A., Hostetler, C. A., Ferrare, R. A., Hair, J. W., Dubey, M. K., Mazzoleni, C., Andrews, E., Coulter, R. L., Lee, Y.-N., Olfert, J., and Springston, S. R.: Overview of the Cumulus Humilis Aerosol Processing Study, Bull. Amer. Meteor. Soc., 90, 1653–1667, doi:10.1175/2009bams2760.1, 2009.

Berg, L. K., Berkowitz, C. M., Barnard, J. C., Senum, G., and Springston, S. R.: Observations of the first aerosol indirect effect in shallow cumuli, Geophys. Res. Lett., 38, L03809, doi:10.1029/2010gl046047, 2011.

Berg, L. K., Gustafson, W. I., Kassianov, E. I., and Deng, L.: Evaluation of a Modified Scheme for Shallow Convection: Implementation of CuP and Case Studies, Mon. Wea. Rev., 141, 134–147, doi:10.1175/mwr-d-12-00136.1, 2013.

Boucher, O., Randall, D. A., Artaxo, P., Bretherton, C. S., Feingold, G., Forster, P., Kerminen, V.-M., Kondo, Y., Liao, H., Lohmann, U., Rasch, P., Satheesh, S. K., Sherwood, S., Stevens, B., and Zhang, X. Y.: Clouds and Aerosols, in: Climate Change 2013: The Physical Science Basis. Contribution of Working Group I to the Fifth Assesment Report to the Intergovernmental Panel on Climate Change, edited by: Stocker, T. F., Qin, D., Plattner, G.-K., Tignor, M., Allen, S. K., Boschung, J., Nauels, A., Xia, Y., Bex, V., and Midgley, P. M., Cambridge University Press, Cambridge, United Kingdom and New York, NY, USA, 2013.

Carter, W. P. L.: SAPRC-99 Mechanism Filess and Associated Programs and Examples, available at: http://www.cert.ucr.edu/~carter/SAPRC99/ (last access: 2 February 2011), last updated 30 March 2010, 2010.

Chapman, E. G., Gustafson Jr., W. I., Easter, R. C., Barnard, J. C., Ghan, S. J., Pekour, M. S., and Fast, J. D.: Coupling aerosol-cloud-radiative processes in the WRF-Chem model: Investigating the radiative impact of elevated point sources, Atmos. Chem. Phys., 9, 945–964, doi:10.5194/acp-9-945-2009, 2009.

Chaumerliac, N., Richard, E., Pinty, J. P., and Nickerson, E. C.: Sulfur scavenging in a mesoscale model with quasi-spectral microphysics: Two-dimensional results for continental and maritime clouds, J. Geophys. Res., 92, 3114–3126, doi:10.1029/JD092iD03p03114, 1987.

Chen, F., Mitchell, K., Schaake, J., Xue, Y., Pan, H.-L., Koren, V., Duan, Q. Y., Ek, M., and Betts, A.: Modeling of land surface evaporation by four schemes and comparison with FIFE observations, J. Geophys. Res., 101, 7251–7268, doi:10.1029/95jd02165, 1996.

Collins, W. D., Rasch, P. J., Boville, B. A., Hack, J. J., McCaa, J. R., Williamson, D. L., Kiehl, J. T., Briegleb, B., Bitz, C., Lin, S.-J., Zhang, M., and Dai, Y.: Description of the NCAR Communtiy Atmosphere Model (CAM 3.0), National Center for Atmospheric Research (NCAR), 214 pp., 2004.

Easter, R. C. and Hobbs, P. V.: The Formation of Sulfates and the Enhancement of Cloud Condensation Nuclei in Clouds, J. Atmos. Sci., 31, 1586–1594, doi:10.1175/1520-0469(1974)031<1586:tfosat>2.0.co;2, 1974.

Eidhammer, T., Barth, M. C., Petters, M. D., Wiedinmyer, C., and Prenni, A. J.: Aerosol microphysical impact on summertime convective precipitation in the Rocky Mountain region, J. Geophys. Res., 119, JD021883, doi:10.1002/2014jd021883, 2014.

Emmons, L. K., Apel, E. C., Lamarque, J.-F., Hess, P. G., Avery, M., Blake, D., Brune, W., Campos, T., Crawford, J., DeCarlo, P. F., Hall, S., Heikes, B., Holloway, J., Jimenez, J. L., Knapp, D. J., Kok, G., Mena-Carrasco, M., Olson, J., O'Sullivan, D., Sachse, G., Walega, J., Weibring, P., Weinheimer, A., and Wiedinmyer, C.: Impact of Mexico City emissions on regional air quality from MOZART-4 simulations, Atmos. Chem. Phys., 10, 6195–6212, doi:10.5194/acp-10-6195-2010, 2010a.

Emmons, L. K., Walters, S., Hess, P. G., Lamarque, J. F., Pfister, G. G., Fillmore, D., Granier, C., Guenther, A., Kinnison, D., Laepple, T., Orlando, J., Tie, X., Tyndall, G., Wiedinmyer, C., Baughcum, S. L., and Kloster, S.: Description and evaluation of the Model for Ozone and Related chemical Tracers, version 4 (MOZART-4), Geosci. Model Dev., 3, 43–67, doi:10.5194/gmd-3-43-2010, 2010b.

Fahey, K. M. and Pandis, S. N.: Optimizing model performance: variable size resolution in cloud chemistry modeling, Atmos.

Environ., 35, 4471–4478, doi:10.1016/S1352-2310(01)00224-2, 2001.

Fan, J., Leung, L. R., Li, Z., Morrison, H., Chen, H., Zhou, Y., Qian, Y., and Wang, Y.: Aerosol impacts on clouds and precipitation in eastern China: Results from bin and bulk microphysics, J. Geophys. Res., 117, D00K36, doi:10.1029/2011jd016537, 2012.

Fast, J. D., Gustafson Jr., W. I., Easter, R. C., Zaveri, R. A., Barnard, J. C., Chapman, E. G., Grell, G. A., and Peckham, S. E.: Evolution of ozone, particulates, and aerosol direct radiative forcing in the vicinity of Houston using a fully coupled meteorology-chemistry-aerosol model, J. Geophys. Res., 111, D21305, doi:10.1029/2005jd006721, 2006.

Gerard, L., Piriou, J.-M., Brožková, R., Geleyn, J.-F., and Banciu, D.: Cloud and Precipitation Parameterization in a Meso-Gamma-Scale Operational Weather Prediction Model, Mon. Wea. Rev., 137, 3960–3977, doi:10.1175/2009mwr2750.1, 2009.

Ghan, S. J. and Easter, R. C.: Impact of cloud-borne aerosol representation on aerosol direct and indirect effects, Atmos. Chem. Phys., 6, 4163–4174, doi:10.5194/acp-6-4163-2006, 2006.

Grell, G. A.: Prognostic Evaluation of Assumptions Used by Cumulus Parameterizations, Mon. Wea. Rev., 121, 764–787, doi:10.1175/1520-0493(1993)121<0764:peoaub>2.0.co;2, 1993.

Grell, G. A. and Dévényi, D.: A generalized approach to parameterizing convection combining ensemble and data assimilation techniques, Geophys. Res. Lett., 29, 38-1–38-4, doi:10.1029/2002gl015311, 2002.

Grell, G. A. and Freitas, S. R.: A scale and aerosol aware stochastic convective parameterization for weather and air quality modeling, Atmos. Chem. Phys., 14, 5233–5250, doi:10.5194/acp-14-5233-2014, 2014.

Grell, G. A., Peckham, S. E., Schmitz, R., McKeen, S. A., Frost, G., Skamarock, W. C., and Eder, B.: Fully coupled "online" chemistry within the WRF model, Atmos. Environ., 39, 6957–6975, doi:10.1016/j.atmosenv.2005.04.027, 2005.

Grell, G. A., Freitas, S. R., Stuefer, M., and Fast, J.: Inclusion of biomass burning in WRF-Chem: impact of wildfires on weather forecasts, Atmos. Chem. Phys., 11, 5289–5303, doi:10.5194/acp-11-5289-2011, 2011.

Guenther, A., Karl, T., Harley, P., Wiedinmyer, C., Palmer, P. I., and Geron, C.: Estimates of global terrestrial isoprene emissions using MEGAN (Model of Emissions of Gases and Aerosols from Nature), Atmos. Chem. Phys., 6, 3181–3210, doi:10.5194/acp-6-3181-2006, 2006.

Gustafson Jr., W. I., Chapman, E. G., Ghan, S. J., Easter, R. C., and Fast, J. D.: Impact on modeled cloud characteristics due to simplified treatment of uniform cloud condensation nuclei during NEAQS 2004, Geophys. Res. Lett., 34, L19809, doi:10.1029/2007gl030021, 2007.

Gustafson, W. I., Qian, Y., and Fast, J. D.: Downscaling aerosols and the impact of neglected subgrid processes on direct aerosol radiative forcing for a representative global climate model grid spacing, J. Geophys. Res., 116, D13303, doi:10.1029/2010jd015480, 2011.

Gustafson, W. I., Ma, P.-L., Xiao, H., Singh, B., Rasch, P. J., and Fast, J. D.: The Separate Physics and Dynamics Experiment (SPADE) framework for determining resolution awareness: A case study of microphysics, J. Geophys. Res., 118, 9258–9276, doi:10.1002/jgrd.50711, 2013.

Hair, J. W., Hostetler, C. A., Cook, A. L., Harper, D. B., Ferrare, R. A., Mack, T. L., Welch, W., Izquierdo, L. R., and Hovis, F. E.: Airborne High Spectral Resolution Lidar for profiling aerosol optical properties, Appl. Opt., 47, 6734–6752, 2008.

Hegg, D. A., Rutledge, S. A., and Hobbs, P. V.: A numerical model for sulfur and nitrogen scavenging in narrow cold-frontal rainbands: 2. Discussion of chemical fields, J. Geophys. Res., 91, 14403–14416, doi:10.1029/JD091iD13p14403, 1986.

Herwehe, J. A., Alapaty, K., Spero, T. L., and Nolte, C. G.: Increasing the credibility of regional climate simulations by introducing subgrid-scale cloud-radiation interactions, J. Geophys. Res., 119, JD021504, doi:10.1002/2014jd021504, 2014.

Hodzic, A., Jimenez, J. L., Madronich, S., Canagaratna, M. R., DeCarlo, P. F., Kleinman, L., and Fast, J.: Modeling organic aerosols in a megacity: potential contribution of semi-volatile and intermediate volatility primary organic compounds to secondary organic aerosol formation, Atmos. Chem. Phys., 10, 5491–5514, doi:10.5194/acp-10-5491-2010, 2010.

Hsu, Y., Strait, R., Roe, S., and Holoman, D.: SPECIATE 4.0: Speciation Database Development Documentation, Final Report, 156 pp., 2006.

Janjić, Z. I.: The Step-Mountain Coordinate: Physical Package, Mon. Wea. Rev., 118, 1429–1443, doi:10.1175/1520-0493(1990)118<1429:tsmcpp>2.0.co;2, 1990.

Janjić, Z. I.: Nonsingular Implementation of the Mellor-Yamada Level 2.5 Scheme in the NCEP Meso model, National Center for Environmental Prediction (NCEP), 61 pp., 2002.

Kain, J. S.: The Kain-Fritsch Convective Parameterization: An Update, J. Applied Meteor., 43, 170–181, doi:10.1175/1520-0450(2004)043<0170:tkcpau>2.0.co;2, 2004.

Kain, J. S. and Fritsch, J. M.: A One-Dimensional Entraining/Detraining Plume Model and Its Application in Convective Parameterization, J. Atmos. Sci., 47, 2784–2802, doi:10.1175/1520-0469(1990)047<2784:aodepm>2.0.co;2, 1990.

Kim, S. W., Barth, M. C., and Trainer, M.: Influence of fair-weather cumulus clouds on isoprene chemistry, J. Geophys. Res., 117, D10302, doi:10.1029/2011jd017099, 2012.

Koch, D., Park, J., and Del Genio, A.: Clouds and sulfate are anticorrelated: A new diagnostic for global sulfur models, J. Geophys. Res., 108, 4781, doi:10.1029/2003jd003621, 2003.

Larson, V. E., Schanen, D. P., Wang, M. H., Ovchinnikov, M., and Ghan, S.: PDF Parameterization of Boundary Layer Clouds in Models with Horizontal Grid Spacings from 2 to 16 km, Mon. Wea. Rev., 140, 285–306, doi:10.1175/mwr-d-10-05059.1, 2012.

Lim, K.-S. S., Fan, J., Ruby Leung, L., Ma, P.-L., Singh, B., Zhao, C., Zhang, Y., Zhang, G., and Song, X.: Investigation of aerosol indirect effects using a cumulus microphysics parameterization in a regional climate model, J. Geophys. Res., JD020958, doi:10.1002/2013jd020958, 2013.

Ma, P. L., Rasch, P. J., Fast, J. D., Easter, R. C., Gustafson Jr, W. I., Liu, X., Ghan, S. J., and Singh, B.: Assessing the CAM5 physics suite in the WRF-Chem model: implementation, evaluation, and resolution sensitivity, Geosci. Model Dev. Discuss., 6, 6157–6218, doi:10.5194/gmdd-6-6157-2013, 2013.

Mashayekhi, R. and Sloan, J. J.: Effects of aerosols on precipitation in north-eastern North America, Atmos. Chem. Phys., 14, 5111–5125, doi:10.5194/acp-14-5111-2014, 2014.

Matsui, H., Koike, M., Kondo, Y., Moteki, N., Fast, J. D., and Zaveri, R. A.: Development and validation of a black carbon mixing state resolved three-dimensional model: Aging processes and radiative impact, J. Geophys. Res., 118, 2304–2326, doi:10.1029/2012jd018446, 2013.

McKeen, S., Chung, S. H., Wilczak, J., Grell, G., Djalalova, I., Peckham, S., Gong, W., Bouchet, V., Moffet, R., Tang, Y., Carmichael, G. R., Mathur, R., and Yu, S.: Evaluation of several PM2.5 forecast models using data collected during the ICARTT/NEAQS 2004 field study, J. Geophys. Res., 112, D10S20, doi:10.1029/2006jd007608, 2007.

Morrison, H., Curry, J. A., and Khvorostyanov, V. I.: A New Double-Moment Microphysics Parameterization for Application in Cloud and Climate Models. Part I: Description, J. Atmos. Sci., 62, 1665–1677, doi:10.1175/jas3446.1, 2005.

Morrison, H., Thompson, G., and Tatarskii, V.: Impact of Cloud Microphysics on the Development of Trailing Stratiform Precipitation in a Simulated Squall Line: Comparison of One- and Two-Moment Schemes, Mon. Wea. Rev., 137, 991–1007, doi:10.1175/2008mwr2556.1, 2009.

Neale, R. B., Chen, C.-C., Gettelman, A., Lauritzen, P. H., Park, S., Williamson, D. L., Conley, A. J., Garcia, R., Kinnison, D., Lamarque, J. F., Marsh, D., Mills, M., Smith, A. K., Tilmes, S., Vitt, F., Morrison, H., Cameron-Smith, P., Collins, W. D., Iacono, M. J., Easter, R. C., Ghan, S. J., Liu, X., Rasch, P. J., and Taylor, M. A.: Description of the NCAR Community Atmosphere Model (CAM 5.0), NCAR, 2012.

Ntelekos, A. A., Smith, J. A., Donner, L., Fast, J. D., Gustafson, W. I., Chapman, E. G., and Krajewski, W. F.: The effects of aerosols on intense convective precipitation in the northeastern United States, Quarterly Journal of the Royal Meteorological Society, 135, 1367–1391, doi:10.1002/qj.476, 2009.

Pfister, G. G., Avise, J., Wiedinmyer, C., Edwards, D. P., Emmons, L. K., Diskin, G. D., Podolske, J., and Wisthaler, A.: CO source contribution analysis for California during ARCTAS-CARB, Atmos. Chem. Phys., 11, 7515–7532, doi:10.5194/acp-11-7515-2011, 2011.

Qian, Y., Gong, D., Fan, J., Leung, L. R., Bennartz, R., Chen, D., and Wang, W.: Heavy pollution suppresses light rain in China: Observations and modeling, J. Geophys. Res., 114, D00K02, doi:10.1029/2008jd011575, 2009.

Saide, P. E., Spak, S. N., Carmichael, G. R., Mena-Carrasco, M. A., Yang, Q., Howell, S., Leon, D. C., Snider, J. R., Bandy, A. R., Collett, J. L., Benedict, K. B., de Szoeke, S. P., Hawkins, L. N., Allen, G., Crawford, I., Crosier, J., and Springston, S. R.: Evaluating WRF-Chem aerosol indirect effects in Southeast Pacific marine stratocumulus during VOCALS-REx, Atmos. Chem. Phys., 12, 3045–3064, doi:10.5194/acp-12-3045-2012, 2012.

Shrivastava, M., Lane, T. E., Donahue, N. M., Pandis, S. N., and Robinson, A. L.: Effects of gas particle partitioning and aging of primary emissions on urban and regional organic aerosol concentrations, J. Geophys. Res., 113, D18301, doi:10.1029/2007jd009735, 2008.

Shrivastava, M., Fast, J., Easter, R., Gustafson Jr., W. I., Zaveri, R. A., Jimenez, J. L., Saide, P., and Hodzic, A.: Modeling organic aerosols in a megacity: comparison of simple and complex representations of the volatility basis set approach, Atmos. Chem. Phys., 11, 6639–6662, doi:10.5194/acp-11-6639-2011, 2011.

Shrivastava, M., Berg, L. K., Fast, J. D., Easter, R. C., Laskin, A., Chapman, E. G., Gustafson, W. I., Liu, Y., and Berkowitz, C. M.: Modeling aerosols and their interactions with shallow cumuli during the 2007 CHAPS field study, J. Geophys. Res., 1343–1360, doi:10.1029/2012JD018218, 2013.

Skamarock, W. C., Klemp, J. B., Dudhia, J., Gill, D. O., Barker, D. M., Duda, M. G., Huang, X.-Y., Wang, W., and Powers, J. G.: A Description of the Advanced Research WRF Version 3, NCARNCAR/TN-475+STR, 2008.

Solomon, S., Qin, D., Manning, M., Alley, R. B., Berntsen, T., Bindoff, N. L., Chen, Z., Chidthaisong, A., Gregory, J. M., Hegerl, G. C., Heimann, M., Hewitson, B., Hoskins, B. J., Joos, F., Jouzel, J., Kattsov, V., Lohmann, U., Matsuno, T., Molina, M., Nicholls, N., Overpeck, J., Raga, G., Ramaswamy, V., Ren, J., Rusticucci, M., Somerville, R., Stocker, T. F., Whetton, P., Wood, R. A., and Wratt, D.: Technical Summary, in: Climate Change 2007: The Physical Science Basis. Contribution of Working Group I to the Fourth Assessment Report of the Intergovernmental Panel on Climate Change, edited by: Solomon, S., Qin, D., Manning, M., Chen, Z., Marquis, M., Averyt, K. B., Tignor, M., and Miller, H. L., Cambridge University Press, Cambridge, United Kingdom and New York, NY, USA, 2007.

Stevens, B. and Feingold, G.: Untangling aerosol effects on clouds and precipitation in a buffered system, Nature, 461, 607–613, 2009.

Stull, R. B.: A fair-weather cumulus cloud classification scheme for mixed-layer studies, J. Climate Appl. Meteor., 24, 49–56, 1985.

Taylor, G. R.: Sulfate Production and Deposition in Midlatitude Continental Cumulus Clouds. Part I: Cloud Model Formulation and Base Run Analysis, J. Atmos. Sci., 46, 1971–1990, doi:10.1175/1520-0469(1989)046<1971:spadim>2.0.co;2, 1989.

Tremblay, A. and Leighton, H.: A Three-Dimensional Cloud Chemistry Model, J. Climate Appl. Meteor., 25, 652–671, doi:10.1175/1520-0450(1986)025<0652:atdccm>2.0.co;2, 1986.

Tsimpidi, A. P., Karydis, V. A., Zavala, M., Lei, W., Molina, L., Ulbrich, I. M., Jimenez, J. L., and Pandis, S. N.: Evaluation of the volatility basis-set approach for the simulation of organic aerosol formation in the Mexico City metropolitan area, Atmos. Chem. Phys., 10, 525–546, doi:10.5194/acp-10-525-2010, 2010.

Vilà-Guerau de Arellano, J., Kim, S.-W., Barth, M. C., and Patton, E. G.: Transport and chemical transformations influenced by shallow cumulus over land, Atmos. Chem. Phys., 5, 3219–3231, doi:10.5194/acp-5-3219-2005, 2005.

Wang, C. and Chang, J. S.: A three-dimensional numerical model of cloud dynamics, microphysics, and chemistry: 1. Concepts and formulation, J. Geophys. Res., 98, 14827–14844, doi:10.1029/92jd01393, 1993.

Wang, H., Rasch, P. J., and Feingold, G.: Manipulating marine stratocumulus cloud amount and albedo: a process-modelling study of aerosol-cloud-precipitation interactions in response to injection of cloud condensation nuclei, Atmos. Chem. Phys. Discuss., 11, 885–916, doi:10.5194/acpd-11-885-2011, 2011.

Wang, H., Easter, R. C., Rasch, P. J., Wang, M., Liu, X., Ghan, S. J., Qian, Y., Yoon, J. H., Ma, P. L., and Vinoj, V.: Sensitivity of remote aerosol distributions to representation of cloud–aerosol interactions in a global climate model, Geosci. Model Dev., 6, 765–782, doi:10.5194/gmd-6-765-2013, 2013.

Wiedinmyer, C., Akagi, S. K., Yokelson, R. J., Emmons, L. K., Al-Saadi, J. A., Orlando, J. J., and Soja, A. J.: The Fire INventory from NCAR (FINN): a high resolution global model to estimate the emissions from open burning, Geosci. Model Dev., 4, 625–641, doi:10.5194/gmd-4-625-2011, 2011.

Wyngaard, J. C.: Toward Numerical Modeling in the "Terra Incognita", J. Atmos. Sci., 61, 1816–1826, doi:10.1175/1520-0469(2004)061<1816:tnmitt>2.0.co;2, 2004.

Zaveri, R. A., Easter, R. C., Fast, J. D., and Peters, L. K.: Model for Simulating Aerosol Interactions and Chemistry (MOSAIC), J. Geophys. Res., 113, D13204, doi:10.1029/2007jd008782, 2008.

Zhang, G. J. and McFarlane, N. A.: Sensitivity of climate simulations to the parameterization of cumulus convection in the Canadian climate centre general circulation model, Atmosphere-Ocean, 33, 407–446, doi:10.1080/07055900.1995.9649539, 1995.

Zhang, Y., Sartelet, K., Wu, S.-Y., and Seigneur, C.: Application of WRF/Chem-MADRID and WRF/Polyphemus in Europe –Part 1: Model description, evaluation of meteorological predictions, and aerosol-meteorology interactions, Atmos. Chem. Phys., 13, 6807–6843, doi:10.5194/acp-13-6807-2013, 2013.

Zhao, C., Liu, X., Ruby Leung, L., and Hagos, S.: Radiative impact of mineral dust on monsoon precipitation variability over West Africa, Atmos. Chem. Phys., 11, 1879–1893, doi:10.5194/acp-11-1879-2011, 2011.

Zhao, C., Chen, S., Leung, L. R., Qian, Y., Kok, J. F., Zaveri, R. A., and Huang, J.: Uncertainty in modeling dust mass balance and radiative forcing from size parameterization, Atmos. Chem. Phys., 13, 10733–10753, doi:10.5194/acp-13-10733-2013, 2013.